NUMERICAL SOLUTION OF THE NEUMANN-KELVIN PROBLEM AND ITS APPLICATION TO SHIP WAVE-RESISTANCE COMPUTATIONS

Wu-ting Tsai*, Yeun-junn Lin* and Ching-chao Liao**

ABSTRACT

Numerical solution of the Neumann-Kelvin problem by the Green's function method is accomplished for the computations of ship wave-resistance. To make the load of computation reasonable, some numerical experimental results are introduced in the present analysis. A computer program based on such mathematical model and numerical simplifications is developed. Two examples calculated for the Wigley model and Series 60 (C_b=0.6), show that the results are satisfactory.

INTEGRAL EQUATION TO BE SOLVED

In this study, the ship is considered to be in steady uniform motion on the free surface of an otherwise calm water of infinite extent. The Cartestian coordinate system o-xyz, moving with steady velocity -U with the ship, is taken as shown in Fig. 1, where the xy-plane coincides with the undisturbed free surface. An irrotational motion of an incompressible, homogeneous and inviscid fluid is assumed. Then the velocity potential $\Phi(x,y,z)$ of a fluid domain V can be written as

$$\Phi(x,y,z) = Ux + \varphi(x,y,z) \qquad (1)$$

---

* Department of Naval Architecture, National Taiwan University

** Engineering School, Chung Cheng Institute of Technology

where $\varphi(x,y,z)$ is the potential of the perturbation due to the ship. When some suitable restrictions are imposed on the geometry and/or the velocity of the ship such that the free-surface boundary conditions are linearized, the perturbation potential φ shall be the solution of the following boundary value problem,

$$\nabla^2\varphi = 0 \qquad \text{in fluid domain V} \qquad (2)$$

$$\frac{\partial\varphi}{\partial n} = -U\vec{n}\cdot\vec{i} \qquad \text{on hull surface S} \qquad (3)$$

$$\frac{\partial^2\varphi}{\partial x^2} + K_0\frac{\partial\varphi}{\partial z} = 0 \qquad K_0 = \frac{g}{U^2} \qquad \text{on calm free surface z=0} \qquad (4)$$

$$\lim_{R\to\infty} = \begin{cases} o(1/R) & x<0 \\ O(1/R) & x>0 \end{cases} \qquad R=(x^2+y^2+z^2)^{1/2} \qquad (5)$$

This is the so-called Neumann-Kelvin problem, which Brard (1971, 1972) dealt with, in the steady wave resistance theory and plays an important role between the linear theory and the exact problem.

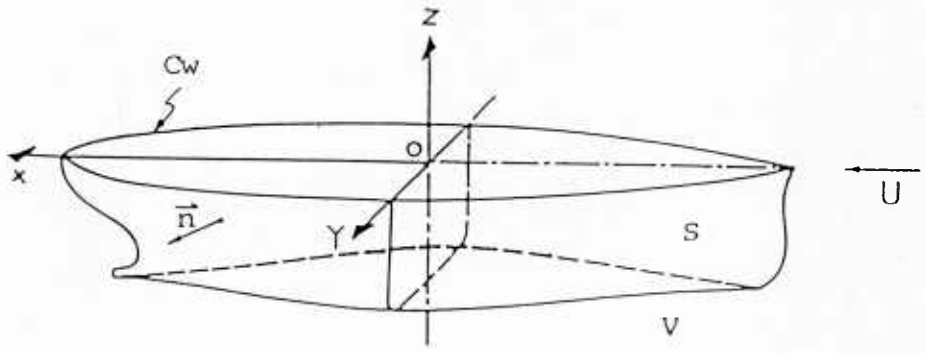

Fig. 1 Coordinate System

The above specific problem may be solved by means of an appropriate Green's function relating to the boundary conditions. The desired function G(P;Q), often known as the Havelock source function or Kelvin source function, is a harmonic function in the fluid domain except having a singularity at Q, and satisfied the linearized free-surface condition and the radiation condition as follows,

$$G(P;Q) = \delta(P;Q) \qquad P,Q\in V \qquad (6)$$

$$\frac{\partial^2 G}{\partial x^2} + K_0 \frac{\partial G}{\partial z} = 0 , \qquad \text{on } z=0 \tag{7}$$

$$\lim_{R\to\infty} G(P;Q) = \begin{cases} o(1/R) & x<0 \\ O(1/R) & x>0 . \end{cases} \qquad R=|P-Q| \tag{8}$$

This yields the expression,

$$G(P;Q) = -\frac{1}{4\pi}\left[\frac{1}{r} \pm \frac{1}{r^*} - I^{\mp}(P;Q)\right], \tag{9}$$

where

$$\begin{cases} r = [(x-\xi)^2+(y-\eta)^2+(z-\zeta)^2]^{1/2} , \\ r^* = [(x-\xi)^2+(y-\eta)^2+(z+\zeta)^2]^{1/2} , \\ I^+ = -4K_0 \int_0^{\frac{\pi}{2}} d\theta \sec^2\theta\, e^{K_0(z+\zeta)\sec^2\theta} \cdot \sin[K_0(x-\xi)\cos\theta]\cdot\cos[K_0(y-\eta)\sin\theta\sec^2\theta] \\ \quad + Re\left\{ \frac{2}{\pi}\int_{-\frac{\pi}{2}}^{\frac{\pi}{2}} d\theta\, P.V. \int_0^{\infty} k \frac{\exp[k(z+\zeta)+ik\tilde{\omega}]}{k-K_0\sec^2\theta} dk \right\} , \\ I^- = -4K_0 \int_0^{\frac{\pi}{2}} d\theta \cdot \sec^2\theta \cdot e^{K_0(z+\zeta)\sec^2\theta} \cdot \sin[K_0(x-\xi)\cos\theta]\cdot\cos[K_0(y-\eta)\sin\theta\sec^2\theta] \\ \quad + Re\left\{ \frac{2K_0}{\pi}\int_{-\frac{\pi}{2}}^{\frac{\pi}{2}} d\theta \sec^2\theta\, P.V. \int_0^{\infty} \frac{\exp[k(z+\zeta)+ik\tilde{\omega}]}{k-K_0\sec^2\theta} dk \right\} , \\ \tilde{\omega} = (x-\xi)\cos\theta + (y-\eta)\sin\theta . \end{cases} \tag{10}$$

By use of such a source function, the Green's second identity gives the perturbation potential φ into the form,

$$\varphi(P) = \iint_S \sigma(Q) G(P;Q)\, ds(Q) - \frac{1}{4\pi K_0}\oint_{C_W} \sigma(Q)\, I^-(P;Q)\, \vec{n}_Q \cdot \vec{i}\, d\eta, \tag{11}$$

where $\sigma(Q)$ is the density of the source distribution to be determined to represent an equivalent flow field. Meanwhile, the Neumann-Kelvin problem can be replaced by the following equation,

$$\begin{aligned} &\frac{1}{2}\sigma(P) + \iint_S \sigma(Q)\frac{\partial G}{\partial n_P}(P;Q)\, ds(Q) \\ &\quad - \frac{1}{4\pi K_0}\oint_{C_W} \sigma(Q)\frac{\partial I^-}{\partial n_P}(P;Q)\vec{n}_Q\cdot\vec{i}\, d\eta = -U\vec{n}_P\cdot\vec{i} , \quad (P\in S\cup C_W) \end{aligned} \tag{12}$$

which is a Fredholm integral equation of the second kind for the unkmown function $\sigma(Q)$ defined over the hull surface S and waterline C_W.

Though other types of integral equation had been derived, e.g., Liao (1973), only the form given by equation (12), i.e., the representation by an equivalent source distribution, will be considered in the present study.

NUMERICAL TREATMENT OF THE INTEGRAL EQUATION

Numerical solution of the integral equation (12) requires an approximate representation of the hull surface S and waterline C_W, and an approximate evaluation of the relevant integration over S and C_W, to discretize the integral equation (12). In the present numerical computations, the hull surface and waterline are approximated by a large number of plane quadrilaterals and line segments respectively. Over each of the elements the source density is assumed to be constant. Thus the integral equation (12) is replaced by a set of linear algebraic equations for those unknown values of source density over the plane and line elements. The source density of the waterline element is assumed to have the same value as that of the plane element adjacent to such line element. With the hull-surface boundary condition being satisfied at the centroid of each plane element, the discrete form of the integral (12) is

$$\frac{1}{2} m_i + \sum_{\substack{j=1 \\ (j\neq i)}}^{N} m_j A_{ij} + \sum_{j=1}^{M} m_j B_{ij} = -\vec{n}_i \cdot \vec{i} \qquad (i=1,2,\ldots.N) \qquad (13)$$

where $m_i (=\sigma_i/U)$ is the nondimensional source density on the i-th element,

n_i is the normal vector of the i-th plane element directed

toward the fluid domain V, and

N is the number of plane elements which approximate the whole hull surface S with the first M elements ending at the waterline.

A_{ij} and B_{ij} are called the influenced coefficient matrices,

$$A_{ij} = \iint_{S_j} \vec{n}_i \cdot \nabla_i G(x_i, y_i, z_i; \xi, \eta, \zeta)\, dS \,, \tag{14}$$

$$B_{ij} = -\frac{1}{4\pi K_0} \int_{C_{wj}} \vec{n}_i \cdot \nabla_i I(x_i, y_i, z_i; \xi, \eta, 0)\, \vec{n}_j \cdot \vec{i}\, d\eta \,, \tag{15}$$

where S_j is the region of the j-th plane element, and

C_{wj} is the region of the j-th line element.

Construction of the influence coefficient matrices A_{ij} and B_{ij} is quite a great numerical work due to the tedious integrations of the kernel function all over the elements representing the hull surface and the waterline. To reduce the extremely long computer time and make the computations practical, one may adopt the numerical experimental results obtained by Lin (1980), and the integration of each kernel function is simplified by the approximations,

$$A_{ij} \cong \frac{\vec{n}_i}{4\pi} \left[-\iint_{S_j} \nabla_i \left(\frac{1}{r} \pm \frac{1}{r^*} \right) dS + a_j \nabla_i I^{\pm}(x_i, y_i, z_i; \xi_{oj}, \eta_{oj}, \zeta_{oj}) \right] \,, \tag{16}$$

$$B_{ij} \cong -\frac{\vec{n}_i}{4\pi K_0} \left[l_j (\vec{n}_j \cdot \vec{i})^2 \cdot \nabla_i I(x_i, y_i, z_i; \xi_{oj}, \eta_{oj}, 0) \right] , \tag{17}$$

where a_j is the area of the j-th plane element,

l_j is the arc length of the j-th line element,

$(\xi_{oj}, \eta_{oj}, \zeta_{oj})$ is the centroid of the j-th plane element, and

$(\xi_{oj}, \eta_{oj}, 0)$ is the midpoint of the j-th line element.

Formulas developed by Hess and Smith (1962, 1964) are used for integrating the kernel of Rankine-source term kernels $\nabla_i(\frac{1}{r} \pm \frac{1}{r'})$. Concentration of constant source density panel as a point source is assumed for the integration of the wavy term kernels $\nabla_i I^{\mp}$.

CALCULATION OF THE DERIVATIVES OF THE HAVELOCK SOURCE FUNCTION

To compute the derivatives of the Havelock source function $\nabla I^{\mp}$ in equations (16) and (17) numerically, the integration contours in complex $k\cos\theta$ plane, as suggested by Noblesse (1977, 1978, 1979) are used to evaluate the principal value double integrals. Fig. 2 is an illustration of the integration contours, which have two poles at $\pm\alpha_0$ and a branch point at $|\beta|$ or $-|\beta|$, where $\alpha = k\cos\theta$, $\beta = k\sin\theta$, and

$$\alpha_0 = \sqrt{\frac{1+(1+4\beta^2)^{1/2}}{2}}$$

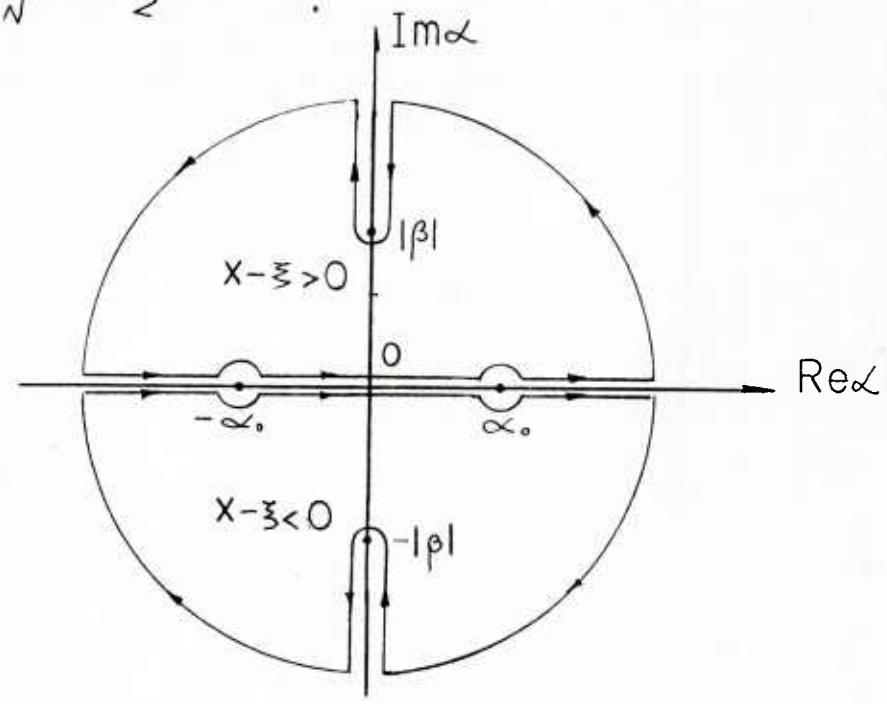

Fig. 2 Integration Contours in Complex α Plane

Via the above scheme, the $\nabla I^{\mp}$ have the following expressions,

$$
\begin{cases}
\dfrac{\partial I^{+}}{\partial x} = -H(x-\xi)\,4K_0^2 \displaystyle\int_{-\pi/3}^{\pi/3} d\theta \cdot \sec^3\theta \cdot \exp[K_0(\beta+\zeta)\cdot\sec^2\theta]\cdot\cos[K_0\tilde{\omega}\sec^2\theta] \\
\qquad + \operatorname{sgn}(x-\xi)\dfrac{2K_0^2}{\pi}\displaystyle\int_{-1}^{1} dt\sqrt{1-t^2}\,\operatorname{Re}\left[e^z E_1(z) - \frac{1}{z} + \frac{1}{z^2}\right], \\
\dfrac{\partial I^{+}}{\partial y} = -H(x-\xi)\,4K_0^2 \displaystyle\int_{-\pi/3}^{\pi/3} d\theta\,\sec^4\theta\cdot\sin\theta\exp[K_0(\beta+\zeta)\sec^2\theta]\cdot\cos[K_0\tilde{\omega}\sec^2\theta] \\
\qquad + \dfrac{2K_0^2}{\pi}\displaystyle\int_{-1}^{1} dt\cdot t\sqrt{1-t^2}\;\operatorname{Im}\left[e^z E_1(z) - \frac{1}{z} + \frac{1}{z^2}\right], \\
\dfrac{\partial I^{+}}{\partial \beta} = -H(x-\xi)\,4K_0^2 \displaystyle\int_{-\pi/3}^{\pi/3} d\theta\,\sec^4\theta\cdot\exp[K_0(\beta+\zeta)\sec^2\theta]\sin[K_0\tilde{\omega}\sec^2\theta] \\
\qquad + \dfrac{2K_0^2}{\pi}\displaystyle\int_{-1}^{1} dt\,(1-t^2)\,\operatorname{Im}\left[e^z E_1(z) - \frac{1}{z} + \frac{1}{z^2}\right],
\end{cases}
\tag{18}
$$

and

$$
\begin{cases}
\dfrac{\partial I^{-}}{\partial x} = -H(x-\xi)\,4K_0^2 \displaystyle\int_{-\pi/3}^{\pi/3} d\theta\cdot\sec^3\theta\cdot\exp[K_0(\beta+\zeta)\cdot\sec^2\theta]\cdot\cos[K_0\tilde{\omega}\sec^2\theta] \\
\qquad + \operatorname{sgn}(x-\xi)\dfrac{2K_0^2}{\pi}\displaystyle\int_{-1}^{1} dt\sqrt{1-t^2}\,\operatorname{Re}\left[e^z E_1(z) - \frac{1}{z}\right], \\
\dfrac{\partial I^{-}}{\partial y} = -H(x-\xi)\,4K_0^2 \displaystyle\int_{-\pi/3}^{\pi/3} d\theta\,\sec^4\theta\sin\theta\exp[K_0(\beta+\zeta)\sec^2\theta]\cdot\cos[K_0\tilde{\omega}\sec^2\theta] \\
\qquad + \dfrac{2K_0^2}{\pi}\displaystyle\int_{-1}^{1} dt\,t\sqrt{1-t^2}\;\operatorname{Im}\left[e^z E_1(z) - \frac{1}{z}\right], \\
\dfrac{\partial I^{-}}{\partial \beta} = -H(x-\xi)\,4K_0^2 \displaystyle\int_{-\pi/3}^{\pi/3} d\theta\,\sec^4\theta\cdot\exp[K_0(\beta+\zeta)\sec^2\theta]\cdot\sin[K_0\tilde{\omega}\sec^2\theta] \\
\qquad + \dfrac{2K_0^2}{\pi}\displaystyle\int_{-1}^{1} dt\,(1-t^2)\,\operatorname{Im}\left[e^z E_1(z) - \frac{1}{z}\right].
\end{cases}
\tag{19}
$$

where $H(x-\xi)$ is the Heavside step function,

$E_1(z) = \int_z^\infty \frac{e^{-t}}{t} dt$ is the complex exponential integral, and

$$Z = k_o\sqrt{1-t^2}\left[(\beta+\zeta)\sqrt{1-t^2} + (y-\eta)t + i|x-\xi|\right] \qquad (20)$$

The principal value double integral has been transformed into a one-fold integral whose integrand contains a complex exponential integral.

Fig. 3.a and Fig. 3.b show the integrands of the first integrals in equations (19) for a particular set of nondimensional variables $k_o(x-\xi)$, $k_o(y-\eta)$ and $k_o(z+\zeta)$. The Simpson's rule is used for such numerical integration. For the integrands of the second integrals in equations (19), Fig. 4.a and Fig. 4.b indicate that the integrands are smooth functions in the integration interval. Gauss-Chebyshev quadrature (using Chebyshev polynominal of the second kind) is used for doing these numerical integrations.

The evaluation of the complex exponential integral $E_1(z)$, $z=u+iv$ is carried out as follows,

for $u^2+v^2 < 5$, the series expansion provided by Abramowitz and Stegun (1964) is used,

$$E_1(z) = -\gamma - \ln z - \sum_{n=1}^{\infty} \frac{(-1)^n z^n}{n \cdot n!} \qquad |\arg z| < \pi \qquad (21)$$

where $\gamma = 0.57721566....$ is the Euler's constant,

for $u^2+v^2 \geq 5$,

$$e^{z}E_1(z) = e^{z}\int_z^{\infty}\frac{e^{-t}}{t}dt$$

$$= \int_0^{\infty} e^{-t}\left[\frac{t+u}{(t+u)^2+v^2}\right]dt + i\int_0^{\infty} e^{-t}\left[\frac{-v}{(t+u)^2+v^2}\right]dt \qquad (22)$$

Gauss-Laguerre quatrature is used to do the numerical integrations of the infinite integrals in equation (22). The computation of complex exponential integral was verified by comparing the results with the tables listed in Abramowtiz and Stegun (1964) PP. 249-251.

COMPUTATIONS OF THE WAVE RESISTANCE

After solving the linear simultaneous equations for the unknown source density, the velocity and the pressure coefficient at the hull surface can be obtained by

$$\nabla\varphi(x_i,y_i,z_i) \cong -\frac{U}{4\pi}\sum_{j=1}^{N} m_j\left[\iint_{S_j}\nabla_i\left(\frac{1}{r}\pm\frac{1}{r^*}\right)ds + a_i\nabla_i I^{\pm}(x_i,y_i,z_i,\xi_{0j},\eta_{0j},\zeta_{0j})\right]$$

$$+\frac{U}{4\pi k_0}\sum_{j=1}^{M} m_j\left[l_j(\vec{n}_j\cdot\vec{i})\cdot\nabla_i I^{-}(x_i,y_i,z_i,\xi_{0j},\eta_{0j},0)\right], \qquad (23)$$

and

$$C_p = 1 - \frac{|U\vec{i}+\nabla\varphi|^2}{U}. \qquad (24)$$

Free surface elevation f(x,y,0) is given by

$$f(x,y,0) = -\frac{g}{U}\frac{\partial\varphi}{\partial x}(x,y,0). \qquad (25)$$

As for the computations of ship wave-resistance, the suggestion of Breslin and King Eng (1963) is adopted. By numerical experimentations, they found that the point sources can replace the panels to give sufficiently accurate calculation of wave resistance. The wave resistance acting upon the ship can be computed most directly by integrating the x-component of the pressure acting on the hull surface,

$$C_p = \frac{R_p}{\frac{1}{2}\rho U^2 S} \cong \sum_{i=1}^{N} C_p (\vec{n}_i \cdot \vec{i}) . \tag{26}$$

An alternative expression of wave resistance can also be derived from the conservation of momentum, and the wave resistance coefficient C_w can be expressed as

$$C_w = \frac{R_w}{\frac{1}{2}\rho U^2 S} = \frac{2\pi}{S} L^2 \int_0^{\pi/2} [C^*(\theta)^2 + S^*(\theta)^2] \, d\theta .$$

$$= \frac{2\pi}{S} L^2 \int_0^{\pi/2} A^*(\theta)^2 \, d\theta \tag{27}$$

where $A^*(\theta)$ is called the weighted amplitude function, and

$$\left.\begin{matrix} C^*(\theta) \\ S^*(\theta) \end{matrix}\right\} = \frac{k_0}{\pi L} \sec^{3/2}\theta \left\{ \iint_S m(\xi,\eta,\zeta) \exp(k_0 \zeta \sec^2\theta) \begin{matrix} \cos \\ \sin \end{matrix} (k_0 \xi \sec\theta) \cos(k_0 \eta \sec^2\theta \cdot \sin\theta) \, dS \right.$$

$$\left. - \frac{1}{k_0} \oint_{C_w} m(\xi,\eta,0) \begin{matrix} \cos \\ \sin \end{matrix} (k_0 \xi \sec\theta) \cos(k_0 \eta \sec^2\theta \cdot \sin\theta) \, \vec{n} \cdot \vec{i} \, d\eta \right\}$$

$$\cong \frac{k_0}{\pi L} \sec^{3/2}\theta \left\{ \sum_{i=1}^{N} m_i a_i \exp(k_0 \zeta_{0i} \sec^2\theta) \begin{matrix} \cos \\ \sin \end{matrix} (k_0 \xi_{0i} \sec\theta) \cdot \cos(k_0 \eta_{0i} \sec^2\theta \sin\theta) \right.$$

$$\left. - \frac{1}{k_0} \sum_{i=1}^{M} m_i l_i (\vec{n}_i \cdot \vec{i}) \begin{matrix} \cos \\ \sin \end{matrix} (k_0 \xi_{0i} \sec\theta) \cdot \cos(k_0 \eta_{0i} \sec^2\theta \cdot \sin\theta) \right\} \tag{28}$$

NUMERICAL RESULTS

Two ship hull forms,the Wigley model and the Series 60, C_b=0.6, are used for numerical solution of the Neumann-Kelvin problem and for the computations of ship wave-resistance. The numerical results include wave resistance coefficients, wave elevations on ship hull side, and weighted amplitude functions. The computations were carried out on the UNIVAC 1100 computer system at the National Taiwan University. Wave resistance coefficients and wave elevations are compared with experimental data and other numerical results which also solving the Neumann-Kelvin problem. Both the experimental data and the numerical results were presented to the "PROCEEDING OF THE WORKSHOP ON SHIP WAVE RESISTANCE COMPUTATIONS, 1979".

Wigley Model For the reason of symmetry, the starboard side of the Wigley model is approximated by 252 plane quadrilateral elements. The results of computation are shown in Table 1 and Fig. 5 to Fig. 15,

Table 1 List of Wave-Resistance Coefficients for Wigley Model,

Fig. 5 Arrangement of Surface Elements for Wigley Model,

Fig. 6 Comparison of Wave-Resistance Coefficients (C_p) with Experimental and Other Numerical Results for Wigley Model,

Fig. 7 Comparison of Wave-Resistance Coefficients (C_w) with Experimental and Other Numerical Results for Wigley Model,

Fig. 8 Comparison of Wave Profile with Experimental and Other Numerical Results for Wigley Model at Fn=0.266,

Fig. 9 Comparison of Wave Profile with Experimental and Other Numerical Results for Wigley Model at Fn=0.348,

Fig. 10 Comparison of Wave Profile with Experimental and Other Numerical Results for Wigley Model at Fn=0.452,

Fig. 11 Amplitude Function of Wigley Model at Fn=0.266,

Fig. 12 Amplitude Function of Wigley Model at Fn=0.313,

Fig. 13 Amplitude Function of Wigley Model at Fn=0.348,

Fig. 14 Amplitude Function of Wigley Model at Fn=0.402,

Fig. 15 Amplitude Function of Wigley Model at Fn=0.452.

Series 60, C_b=0.6 The starboard side hull surface is meshed into 325 plane elements and the numerical results are illustrated in Table 2 and Fig. 16 to Fig. 31,

Table 2 List of Wave-Resistance Coefficients for Series 60, C_b=0.6,

Fig. 16 Arrangement of Surface Elements of Fore Body for Series 60, C_b=0.6,

Fig. 17 Arrangement of Surface Elements of Aft Body for Series 60, C_b=0.6,

Fig. 18 Comparison of Wave-Resistance Coefficients (Cp) with Experimental and Other Numerical Results for Series 60, C_b=0.6,

Fig. 19 Comparison of Wave-Resistance Coefficients (Cw) with Experimental and Other Numerical Results for Series 60, C_b=0.6,

Fig. 20 Comparison of Wave Profile with Experimental and Other Numerical Results for Series 60, C_b=0.6 at Fn=0.22,

Fig. 21 Comparison of Wave Profile with Experimental Results for Series 60, C_b=0.6 at Fn=0.25,

Fig. 22 Comparison of Wave Profile with Experimental and Other Numerical Results for Series 60, C_b=0.6 at Fn=0.28,

Fig. 23 Comparison of Wave Profile with Experimental and Other Numerical Results for Series 60, C_b=0.6 at Fn=0.30,

Fig. 24 Comparison of Wave Profile with Experimental and Other Numerical Results for Series 60, C_b=0.6 at Fn=0.32,

Fig. 25 Comparison of Wave Profile with Experimental and Other Numerical Results for Series 60, C_b=0.6 at Fn=0.35,

Fig. 26 Amplitude Function of Series 60, C_b=0.6 at Fn=0.22,

Fig. 27 Amplitude Function of Series 60, C_b=0.6 at Fn=0.25,

Fig. 28 Amplitude Function of Series 60, C_b=0.6 at Fn=0.28,

Fig. 29 Amplitude Function of Series 60, C_b=0.6 at Fn=0.30,

Fig. 30 Amplitude Function of Series 60, C_b=0.6 at Fn=0.32,

Fig. 31 Amplitude Function of Series 60, C_b=0.6 at Fn=0.35.

CONCLUDING REMARKS

"Neumann-Kelvin problem approach" is used as the mathematical model in the present computations. Two essential points can be concluded for the numerical scheme:

1) Concentration of the source panels as point sources is applied for the approximate integration of the wavy term kernels, and for the computations of the wave resistance.

2) The source density of each waterline element is assumed to be identical with that of the plane element ending at such line element.

Two ship hull forms, the Wigley Model and Series 60, C_b=0.6, are used for the numerical calculation. The numerical results are satisfactory for both two ship hull forms. The following conclusions can be obtained from the numerical results :

1) By use of both wave resistance coefficients and wave profiles, one cannot judge that whether the waterline integral terms plays an important role for the numerical analysis of the Neumann-Kelvin problem or not.

2) For both of the two methods for computing the wave resistance, pressure integration, and amplitude function approach, the results show no significant difference, yet the pressure integration scheme has less hump-hollow phenomenon.

ACKNOWLEDGMENTS

The authers wish to express their sincere gratitude to Professor Wei-yuan Hwang for reviewing the manuscript and useful comments.

REFERENCES

Abramowitz, M. and Stegun, I. A., "HANDBOOK OF MATHEMATICAL FUNCTIONS," Dover Publications, New York, 1964.

Brard, R., "The Neumann-Kelvin Problem for Surface Ships," Report 11 CST., Bassin d'Essais des Carenes, Paris, Jan. 1971.

Brard, R., "The Representation of a Given Ship Form by Singularity Distributions When the Boundary Condition on the Free Surface is Linearized," Journal of Ship Research, Vol. 16, March 1972, pp. 79-92.

Breslin, J. P. and King Eng, "Calculation of the Wave Resistance," Proc. Int. Seminar on Theoretical Wave Resistance, Ann Arbor, Michign, 1963, pp.1083-1110.

Guevel, P. , Delhommeau, G. and Cordonnier, J. P., "Numerical Solution of Neumann-Kelvin Problem by the Method of Singularities," Proc. Second Int. Conf. Numerical Ship Hydrodynamics, Berkeley, CaliF., pp.107-123.

Hess, J. L. and Smith, A. M. O., "Calculation of Non-lifting Potential Flow About Arbitry Three-Dimensional Bodies," Douglas Aircraft Co., Inc. , Report No. E.S. 40622, March 1962.

Hess, J. L. and Smith, A. M. O., "Calculation of Potential Flow About Arbitrary Three-Dimensional Bodies," Journal of Ship Research, Vol. 8, No. 2, 1964, pp.22-44.

Liao, C. C., "On the Potential Theory Applied to the Steady Ship Wave Problem," Doctoral Thesis, Department of Naval Architecture, The University of Tokoy, Dec. 1973.

Lin, Y. J., "Evaluation of Resistance Increment Due to Propeller and Its Application to Aft-Part Hull Form Design," Doctoral Thesis, Department of Naval Architecture, The University of Tokoy, June 1980.

Noblesse, F., "The Fundamental Solution in the Theory of Steady Motion of a Ship," Journal of Ship Research, Vol. 21, No. 2 , June 1977. pp.82-88.

Noblesse, F., "On the Fundamental Function in the Theory of Steady Motion of Ships," Journal of Ship Research, Vol. 22, No. 4, Dec. 1978, pp. 212-215.

Noblesse, F., "Alternative Expressions for the Green Function of the Theory of Ship Wave Resistance," MIT Sea Grant College Program, Report No. MITSG 79-23, Sept. 1979.

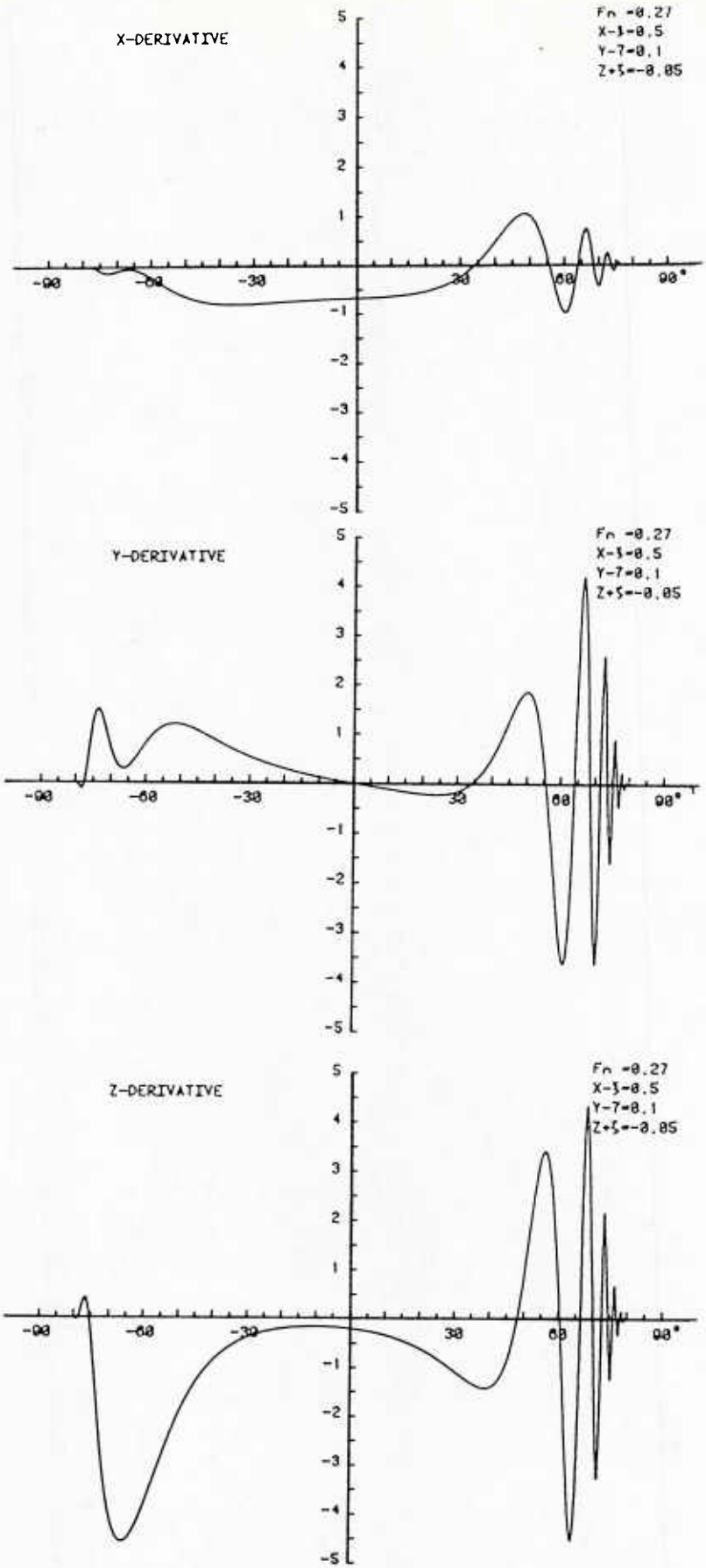

Fig. 3.a Integrands of the First Integrals in Equations (19)

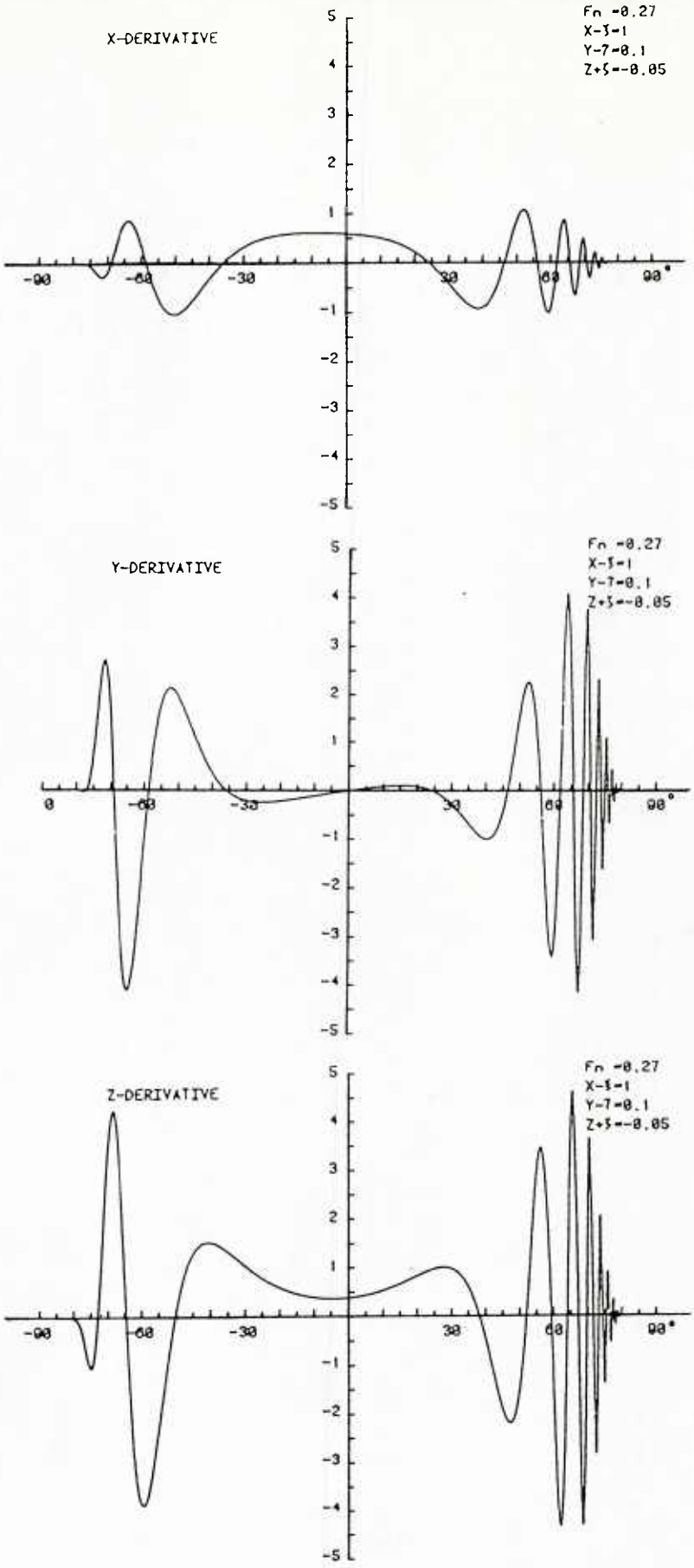

Fig. 3.b Integrands of the First Integrals in Equations (19)

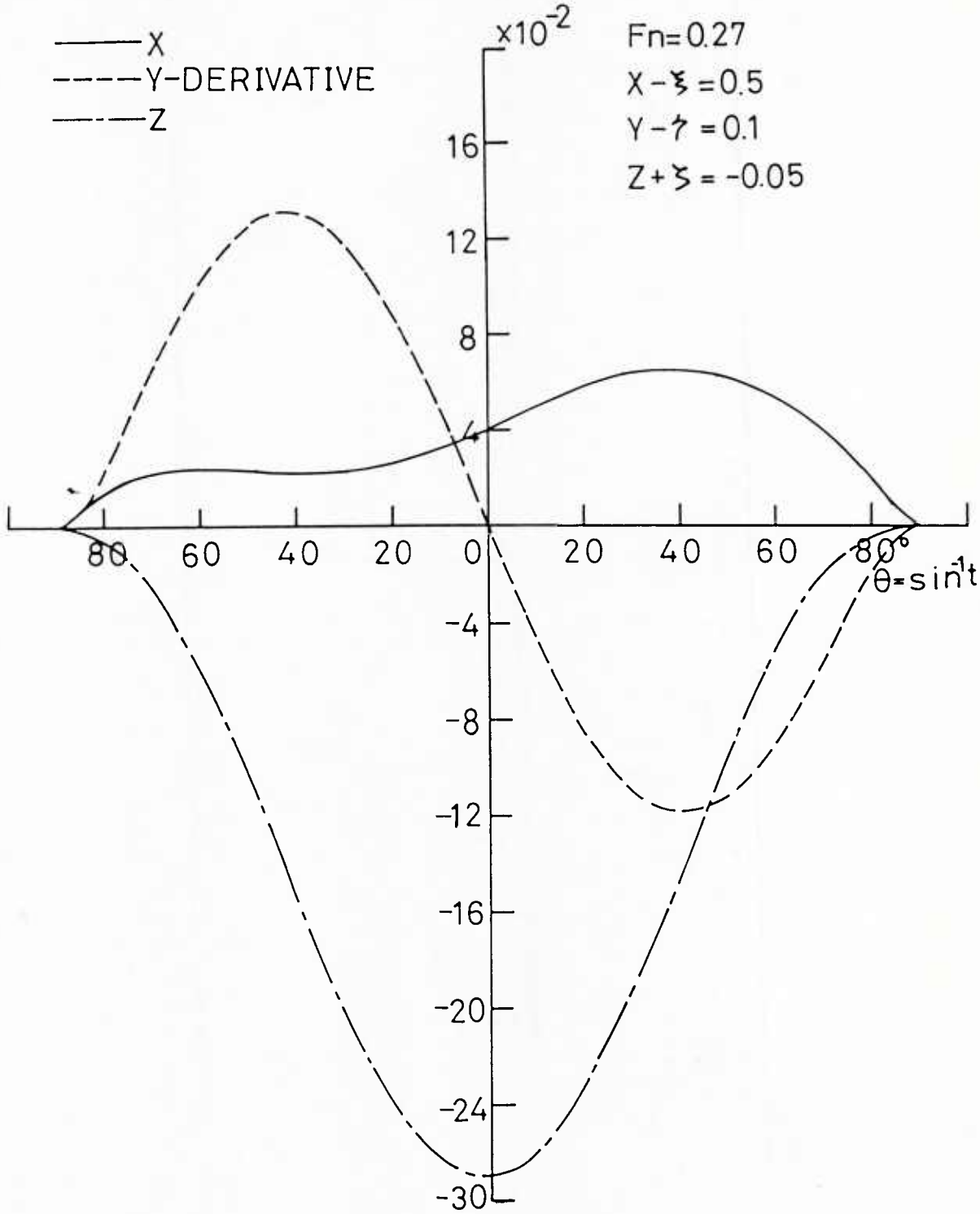

Fig. 4.a Integrands of the Second Integrals in Equations (19)

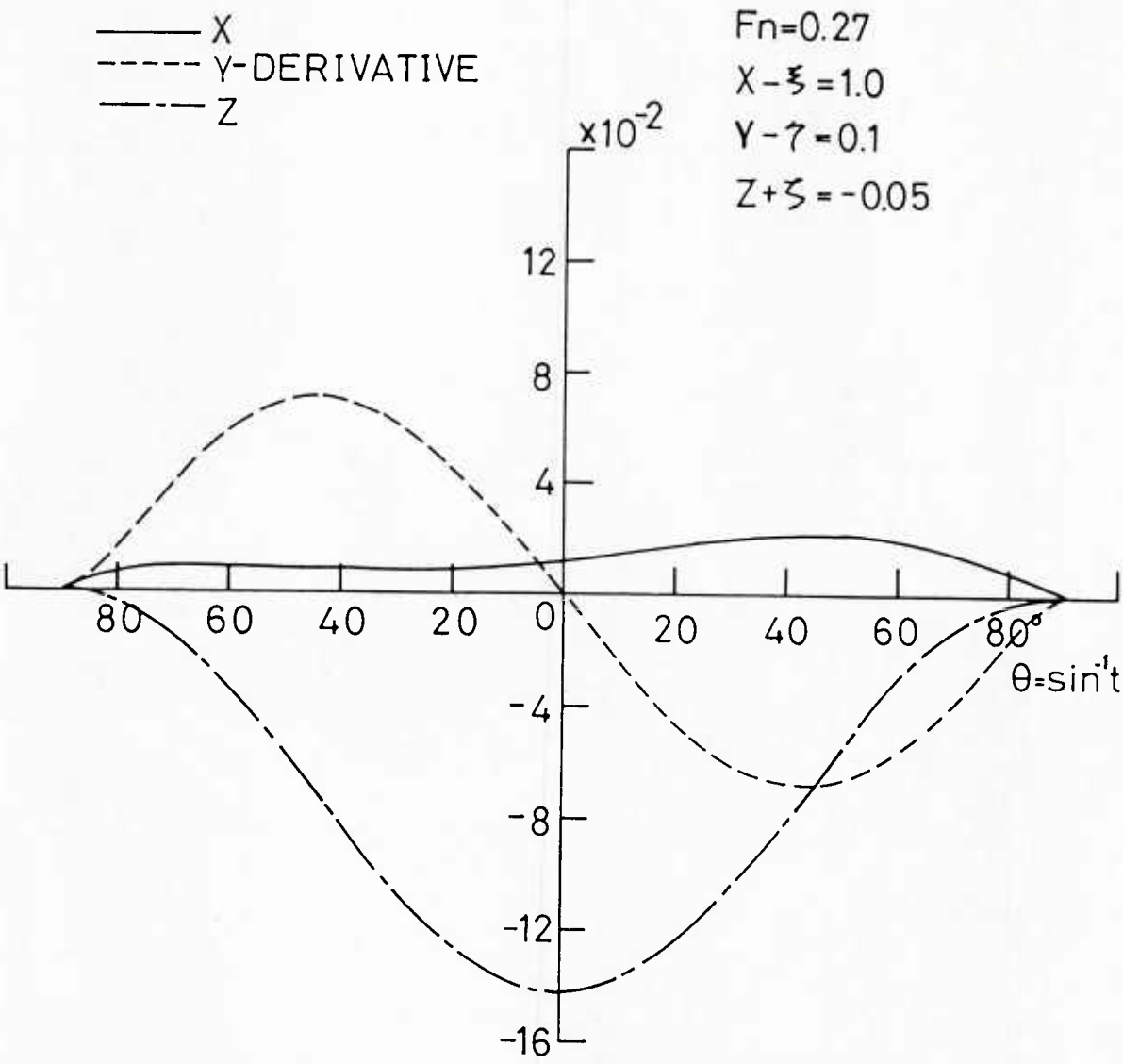

Fig. 4.b Integrands of the Second Integrals in Equations (19)

	Fn	Cw X 10^3				Cp X 10^3	
		Thin Ship Theory	Double Model	Not Consider WL. Int.	Consider WL. Int.	Not Consider WL. Int.	Consider WL. Int.
	0.22	0.6534	0.8166	0.6147	0.5106	0.8584	0.5406
	0.25	1.0641	1.2643	0.7942	0.9539	1.1591	0.9470
*	0.266	0.9458	1.2533	0.7663	0.9319	1.1282	0.9922
	0.27	1.0881	1.4582	0.8216	0.9850	1.1964	1.0427
	0.28	1.6056	2.0936	1.0601	1.2793	1.4450	1.2600
	0.30	2.1441	2.7003	1.3841	1.9181	1.7825	1.7238
*	0.313	1.9133	2.4161	1.3594	2.0893	1.7326	1.7659
	0.32	1.7136	2.1873	1.3128	2.0328	1.6659	1.7222
	0.348	1.2396	1.7033	1.1224	1.4550	1.5119	1.3972
*	0.35	1.2475	1.7230	1.1234	1.4342	1.5170	1.3879
	0.36	1.3738	1.9118	1.1937	1.3976	1.5977	1.3680
	0.40	2.7273	3.5226	1.9042	2.0685	2.2509	1.8269
*	0.452	4.1797	5.1244	2.9703	2.9320	3.1947	2.8368

(* is the recommended Froude number for computations

by 1979 WORKSHOP ON SHIP WAVE-RESISTANCE COMPUTATIONS)

Table 1 List of Wave-Resistance Cefficients for Wigley Model

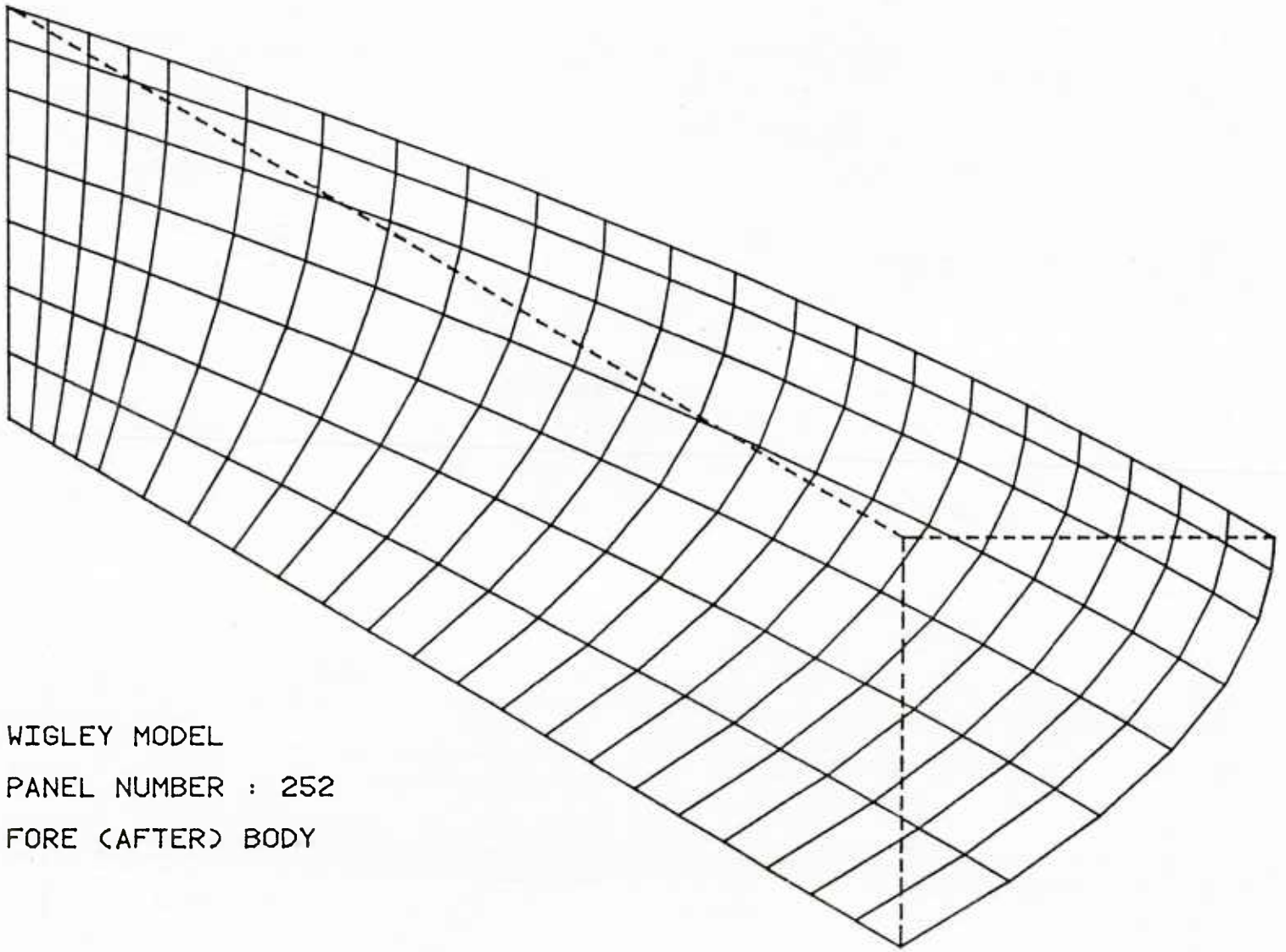

Fig. 5 Arangement of Surface Elements for Wigley Model

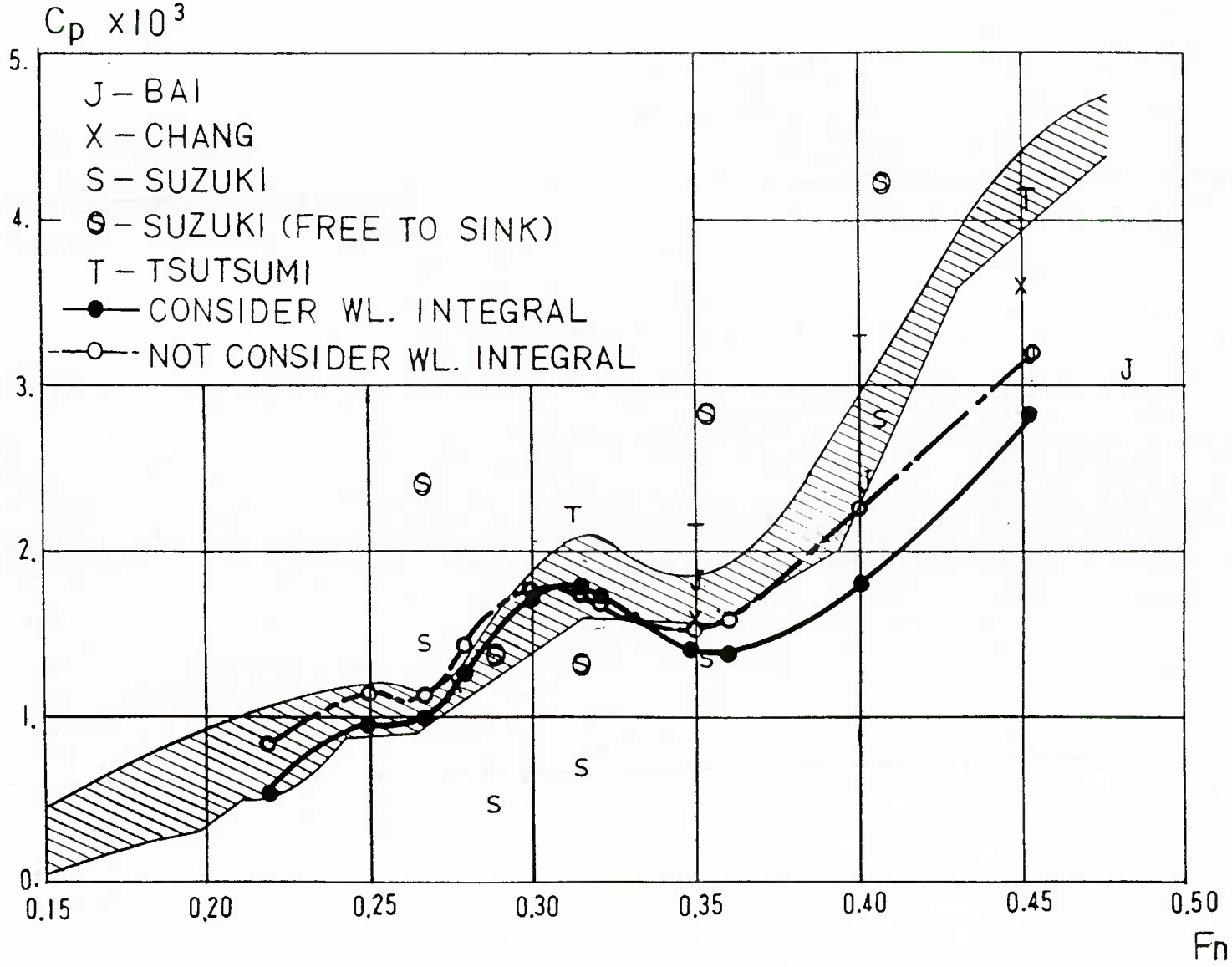

Fig. 6 Comparison of Wave-Resistances (Cp) with Experimental and Other Numerical Results for Wigley

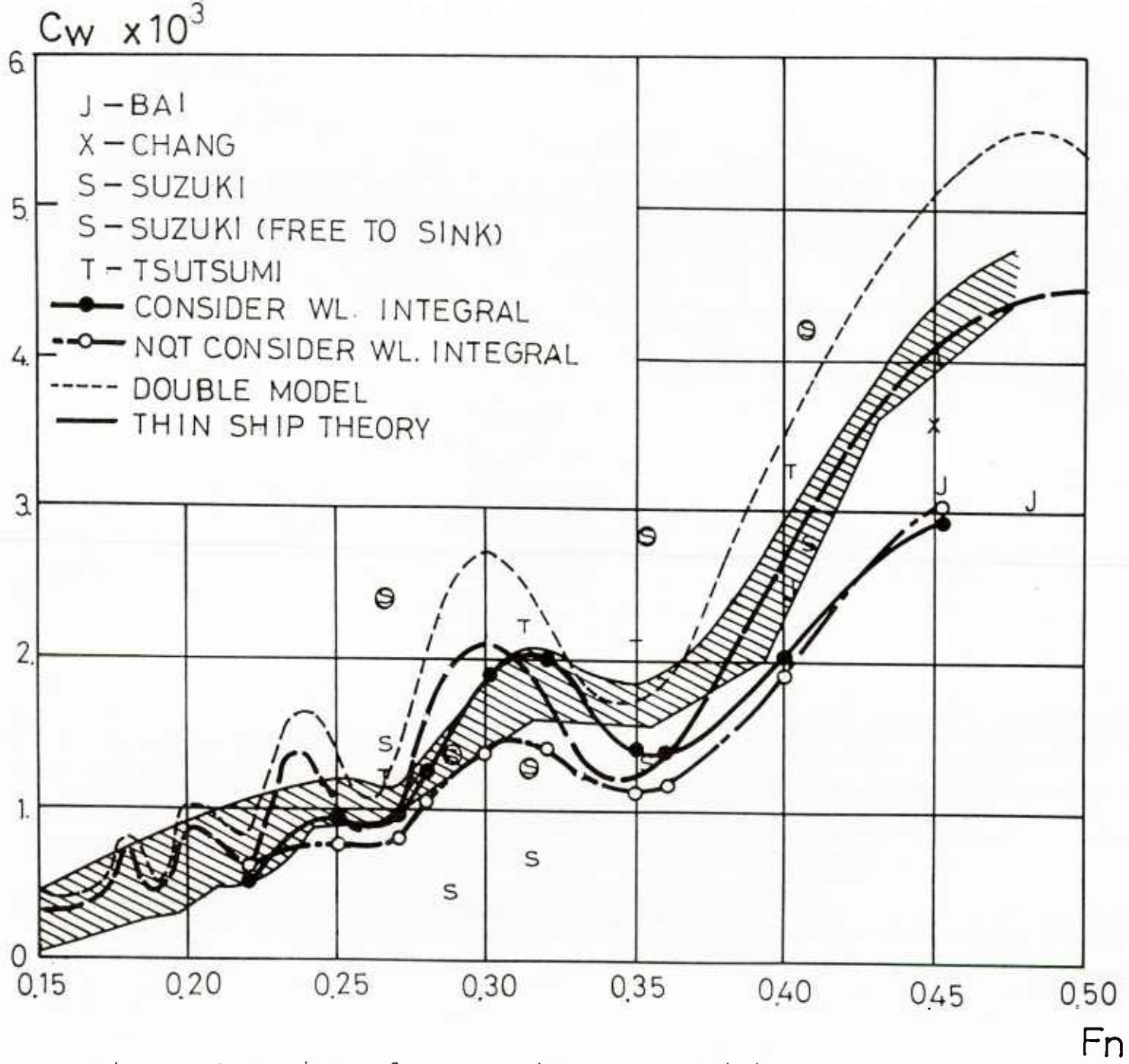

Fig. 7 Comparison of Wave-Resistance Coefficients (Cw) with Experimental and Other Numerical Results for Wigley Model

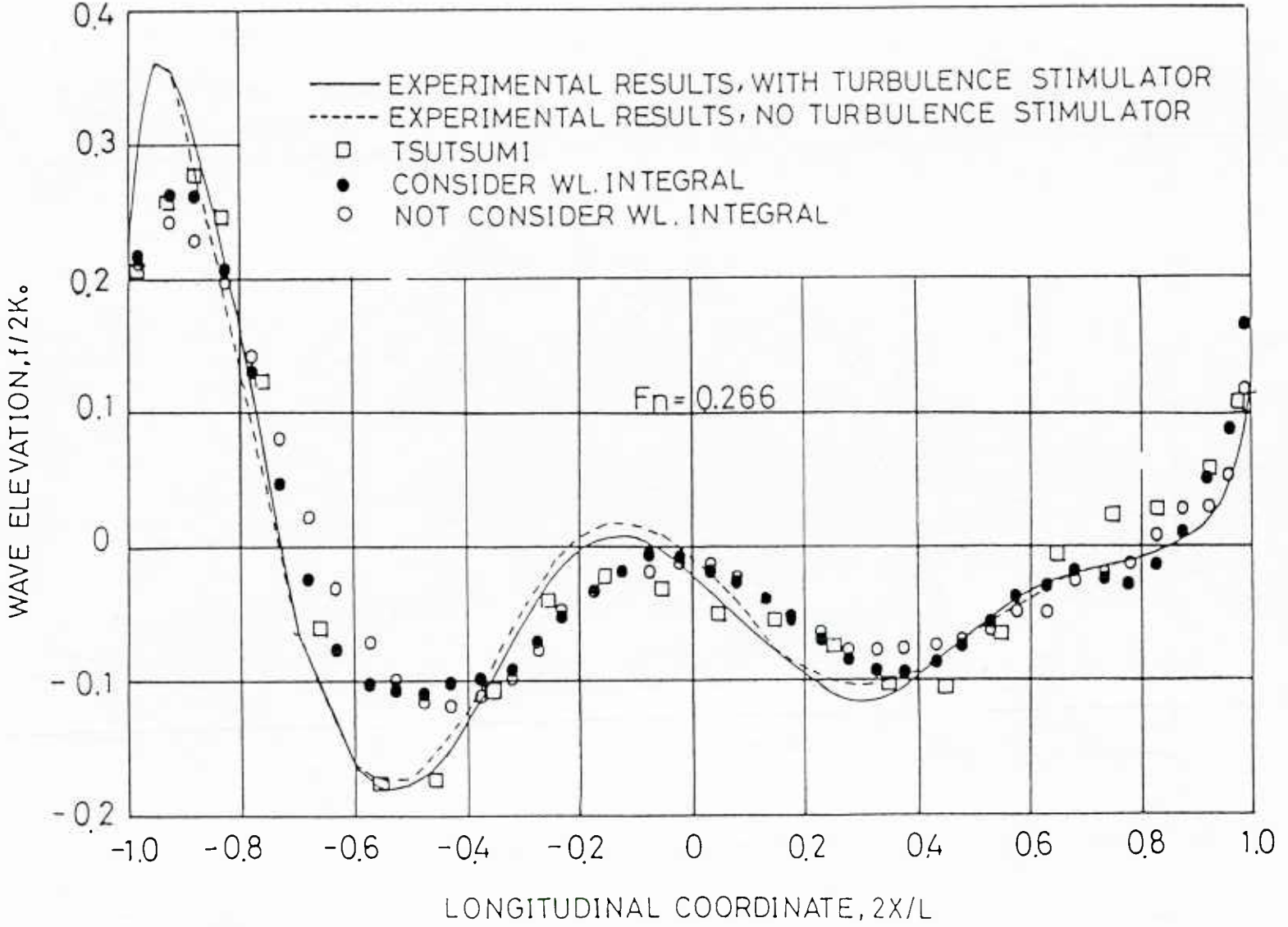

Fig. 8 Comparison of Wave Profile with Experimental and Other Numerical Results for Wigley Model at Fn=0.266

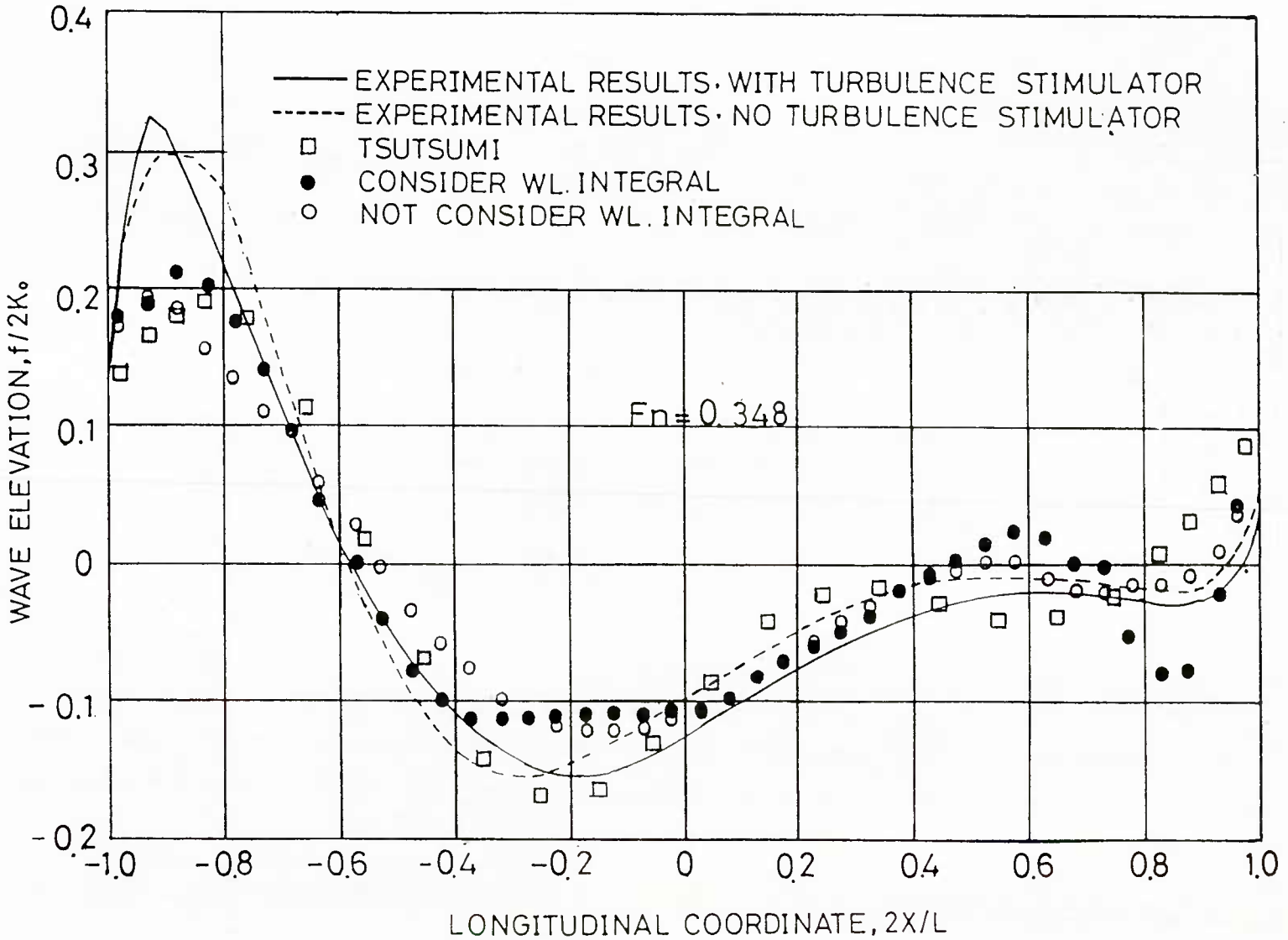

Fig. 9 Comparison of Wave Profile with Experimental and Other Numerical Results for Wigley Model at Fn=0.348

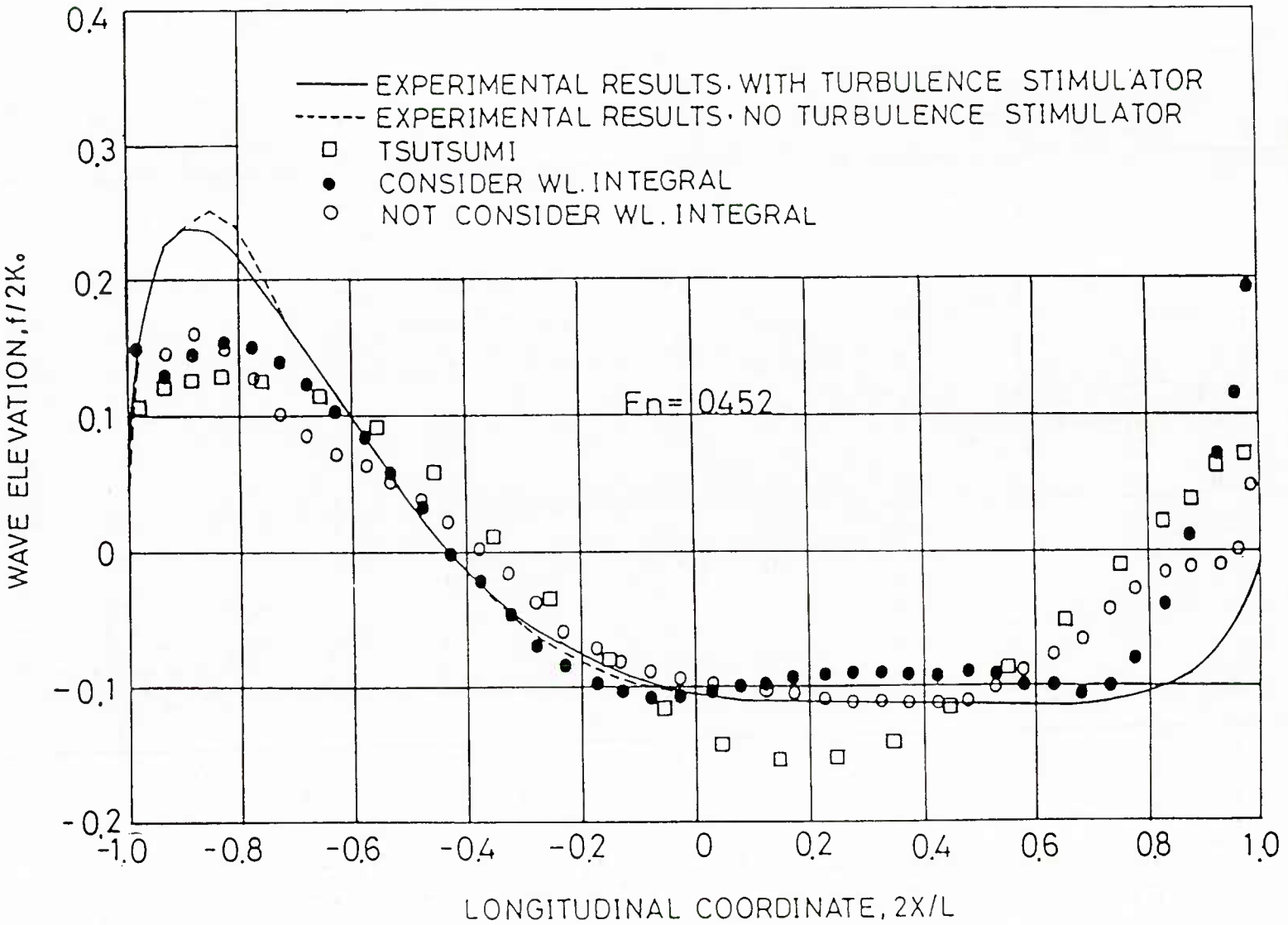

Fig. 10 Compariso of Wave Profile with Experimental and Other Numerical Results for Wigley Model at Fn=0.452

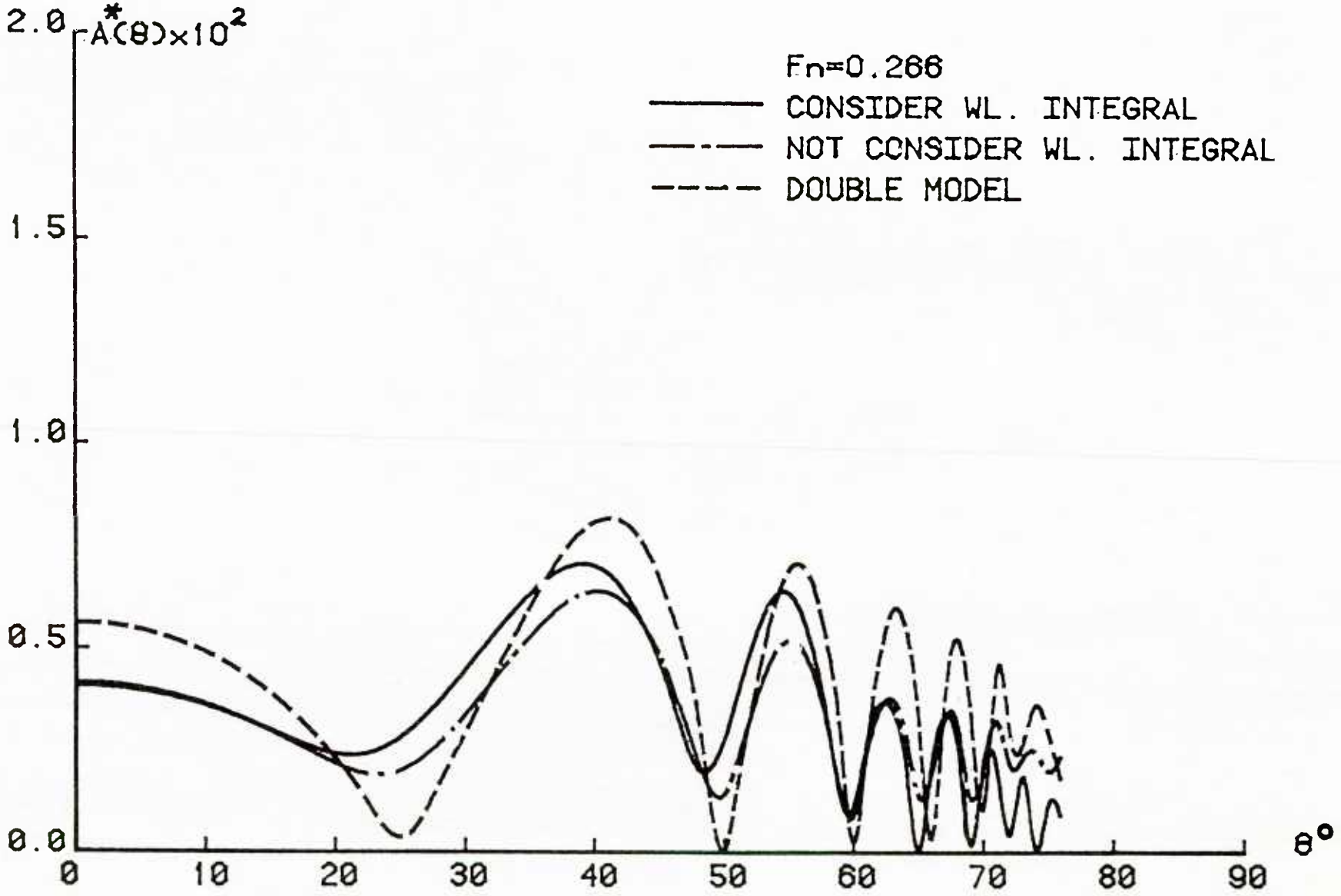

Fig. 11 Amplitude Function of Wigley Model at Fn=0.266

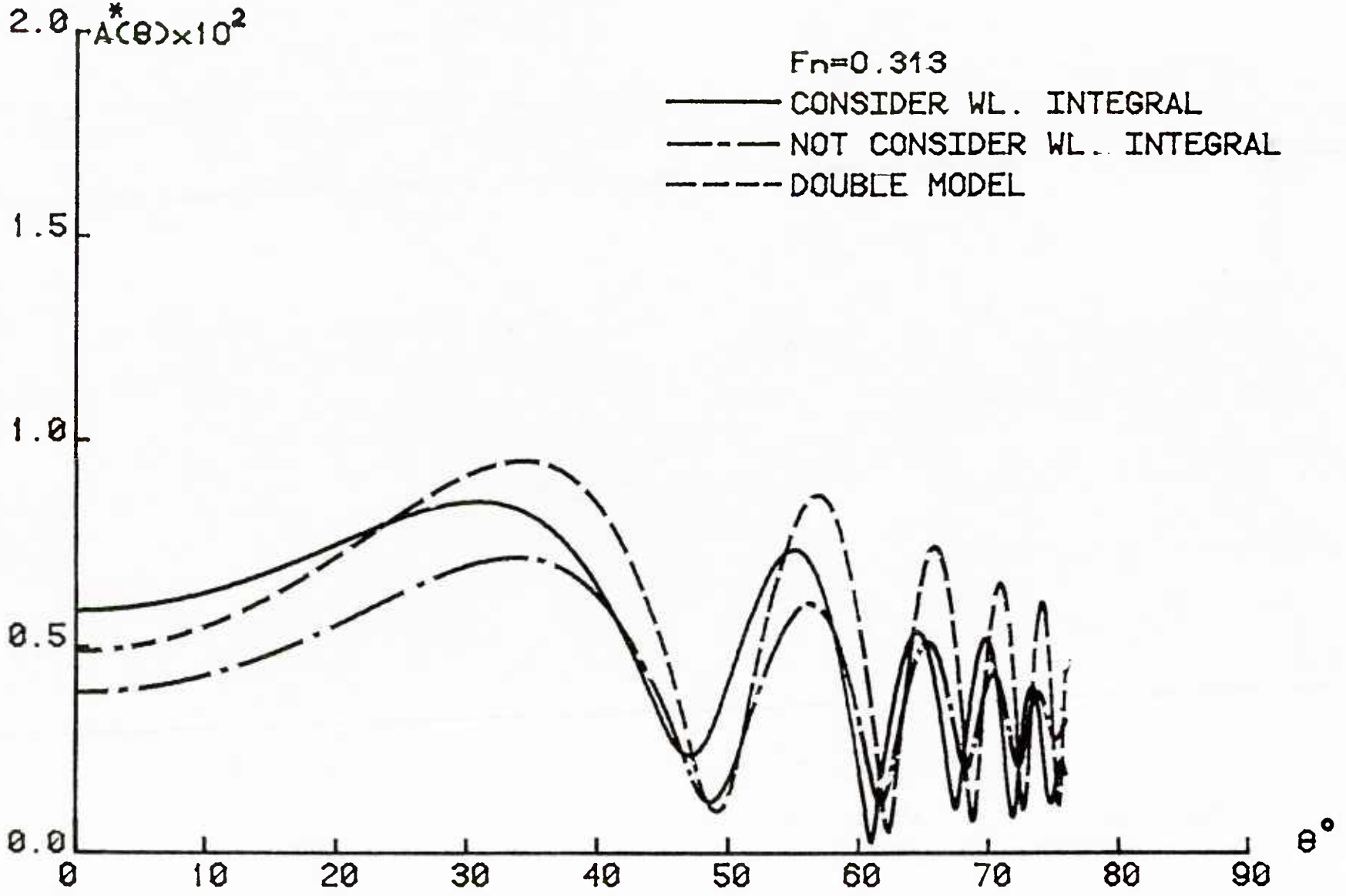

Fig. 12 Amplitude Function of Wigley Model at Fn=0.313

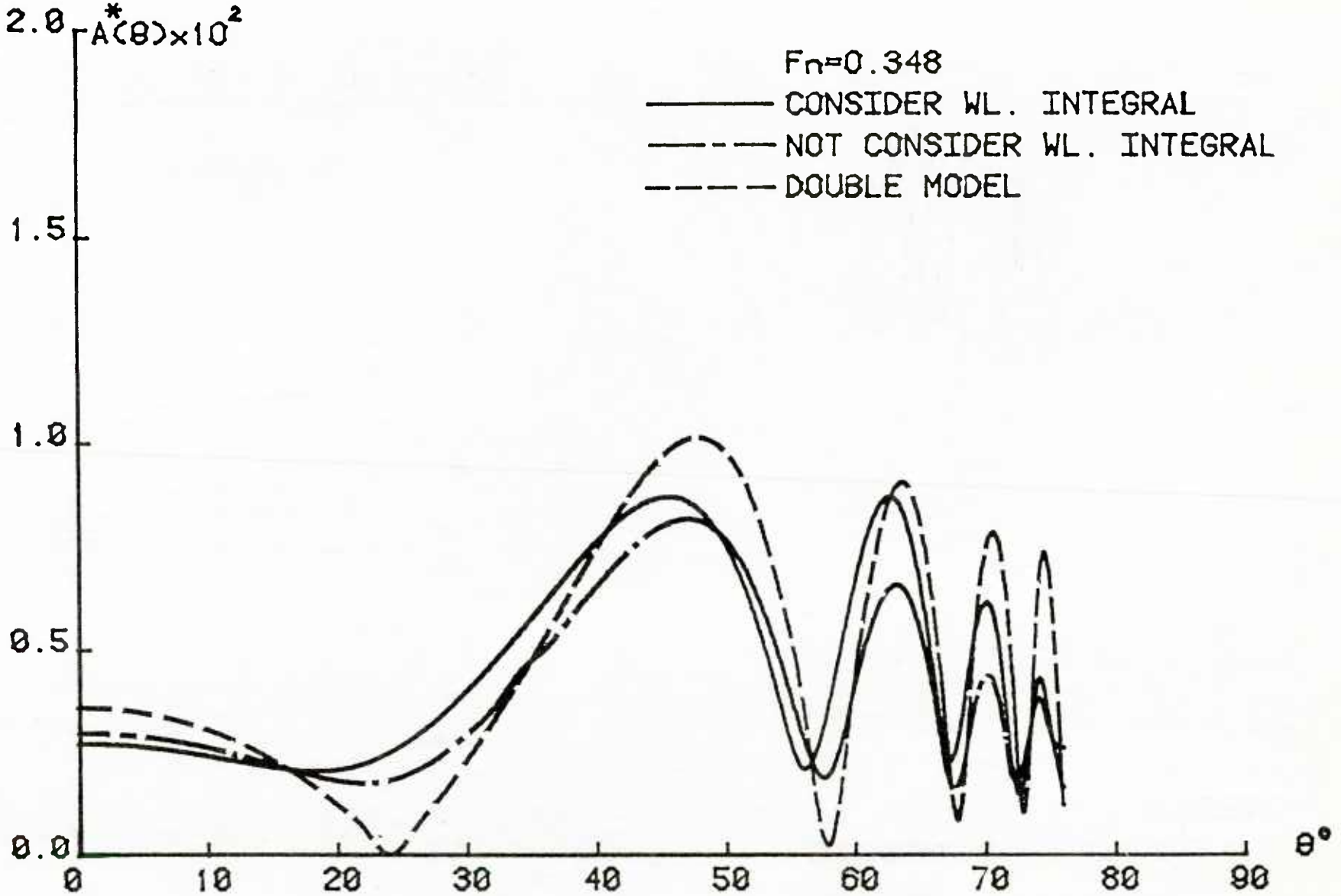

Fig. 13 Amplitude Function of Wigley Model at Fn=0.348

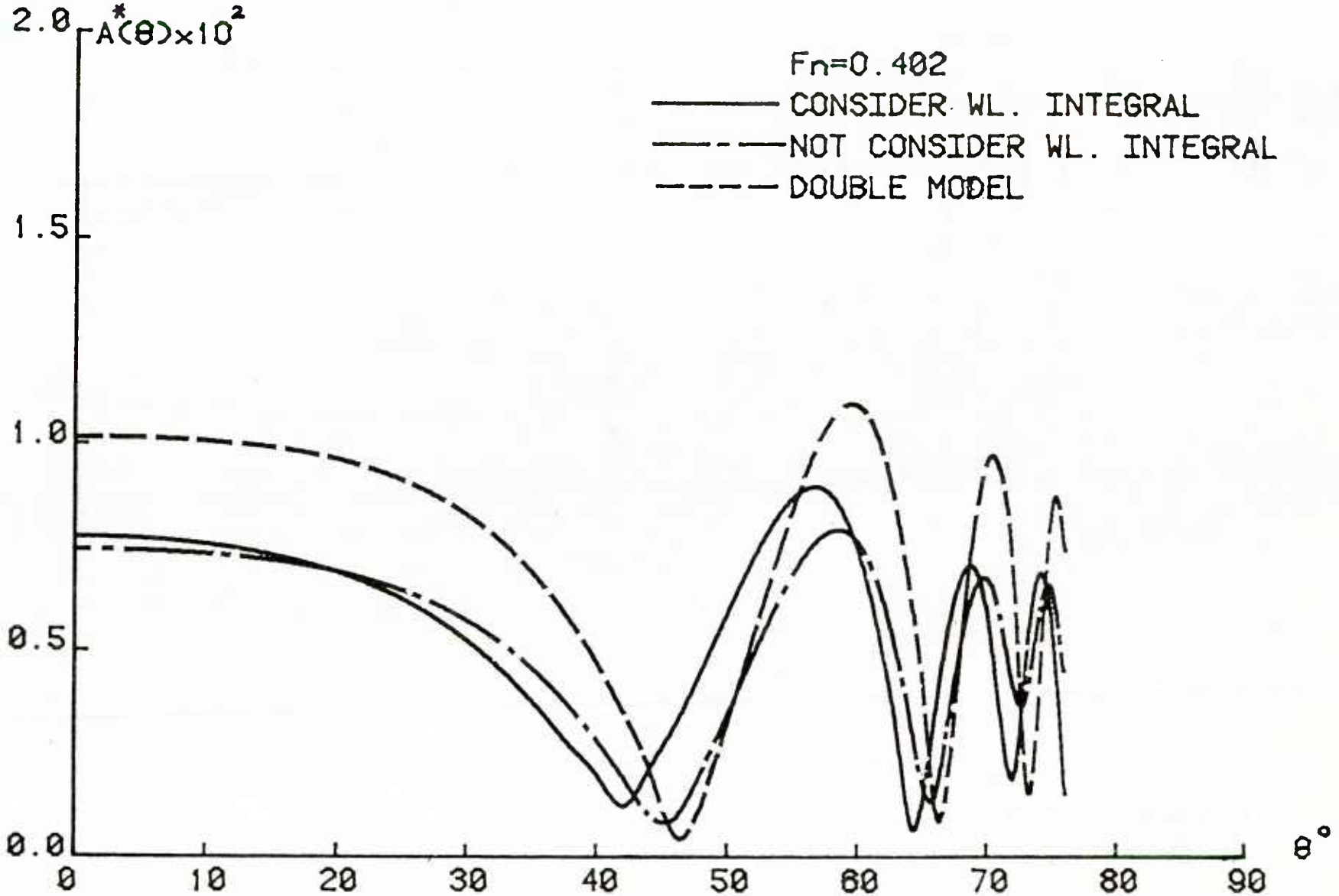

Fig. 14 Amplitude Function of Wigley Model at Fn=0.402

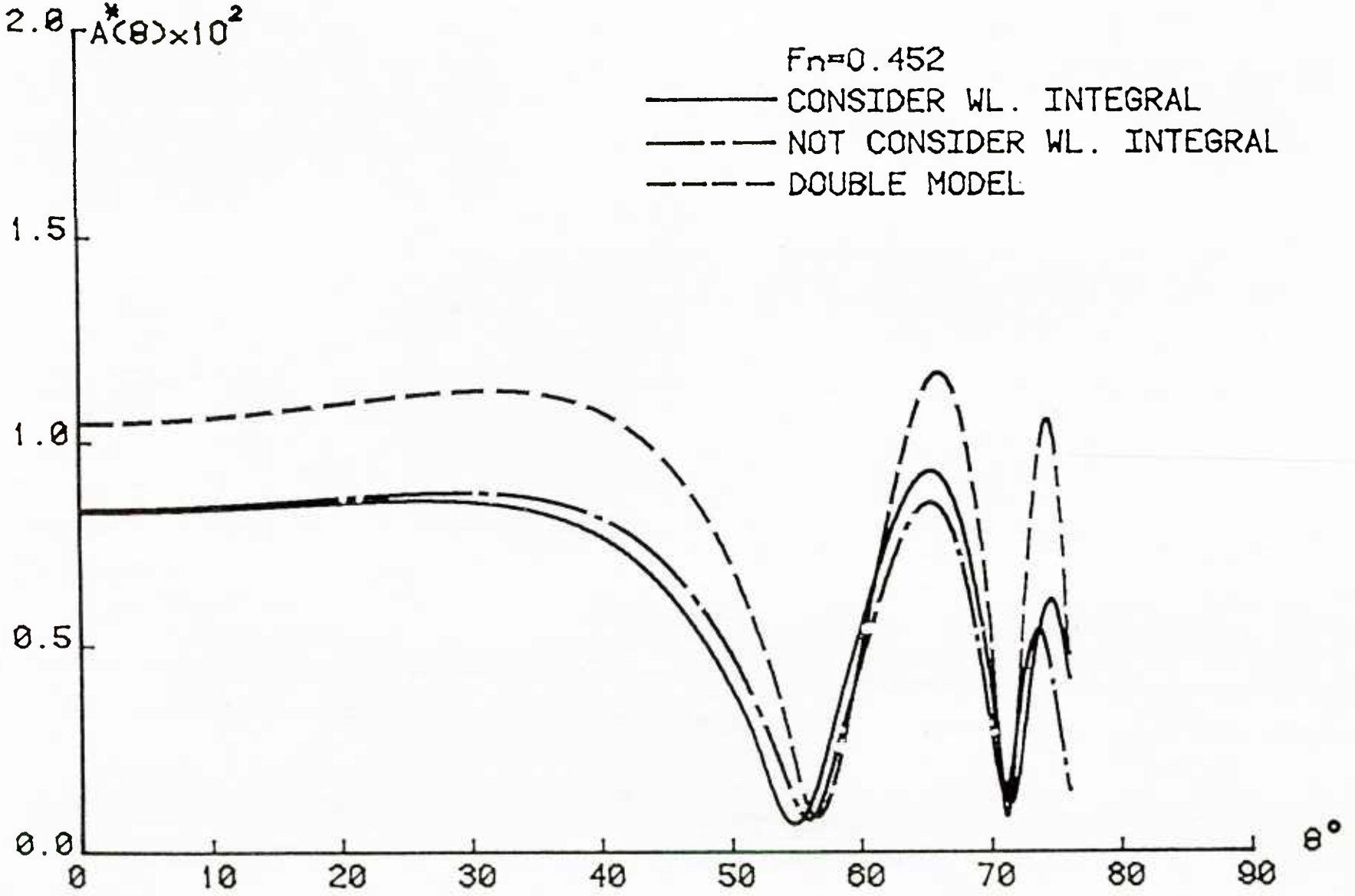

Fig. 15 Amplitude Function of Wigley Model at Fn=0.452

Fn	Cw x 10^3			Cp x 10^3	
	Double Model	Not Consider WL. Int.	Consider WL. Int.	Not Consider WL. Int.	Consider WL. Int.
* 0.22	0.8082	0.4589	0.6564	0.3832	0.6202
* 0.25	1.9467	0.7746	0.8499	0.8256	0.9309
0.27	5.2291	1.5946	1.7144	1.8095	1.6880
* 0.28	6.1652	1.8988	2.3190	2.1439	2.0995
0.30	5.6534	2.0969	2.4007	2.4694	2.4374
* 0.32	4.4869	2.1081	2.1400	2.3681	2.3984
0.35	5.9109	2.6239	2.5661	2.9302	2.9905
0.36	7.1298	3.0550	3.0553	3.4592	3.4263

(* is the recommended Froude number for computations

by 1979 WORKSHOP ON SHIP WAVE-RESISTANCE COMPUTATIONS)

Table 2 List of Wave-Resistance Coefficients for Series 60, Cb=0.6

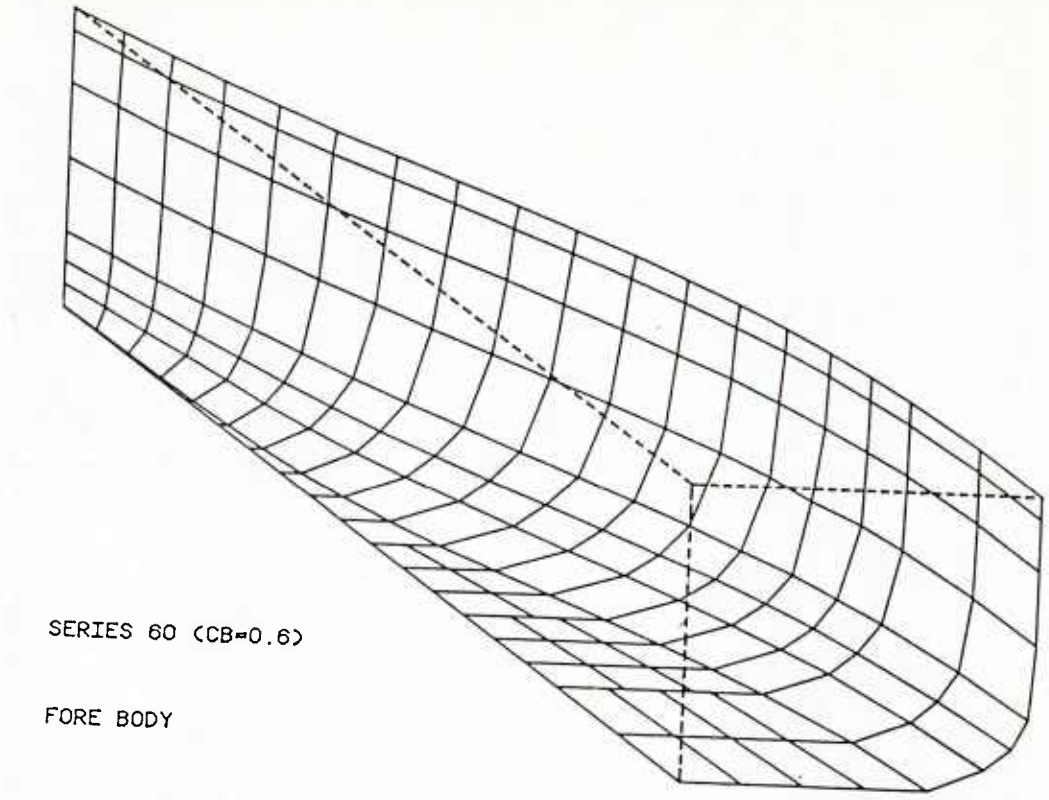

Fig. 16 Arrangement of Surface Elements of Fore Body for Series 60, C_b=0.6

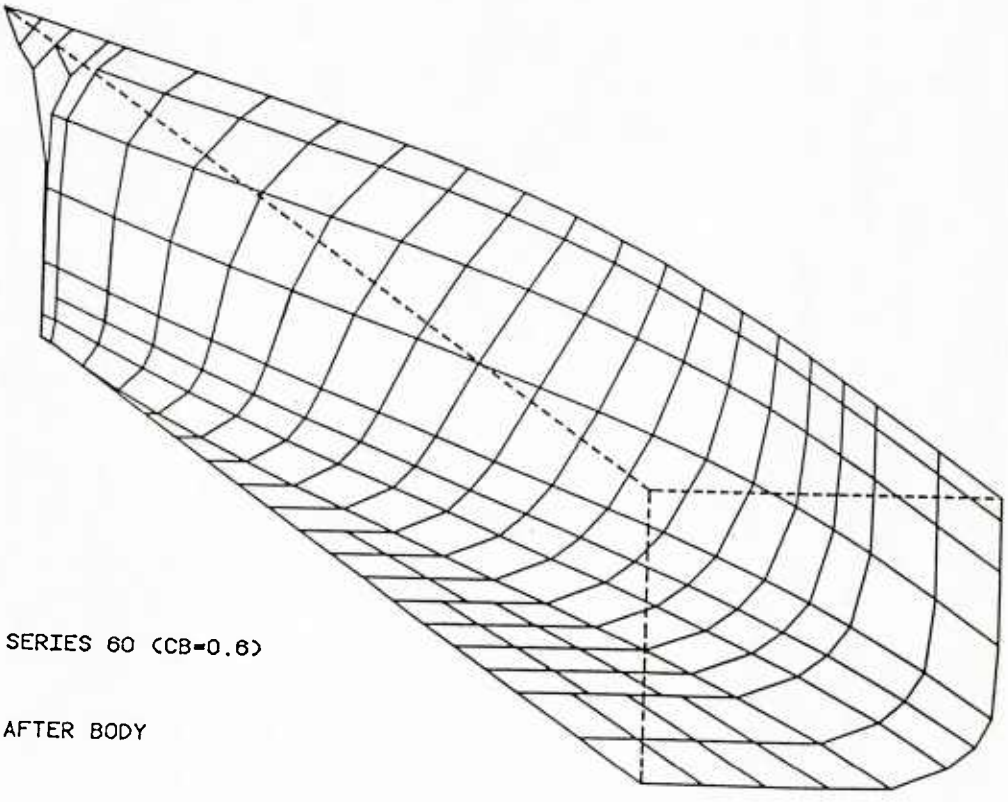

Fig. 17 Arrangement of Surface Elements of Aft Body for Series 60, C_b=0.6

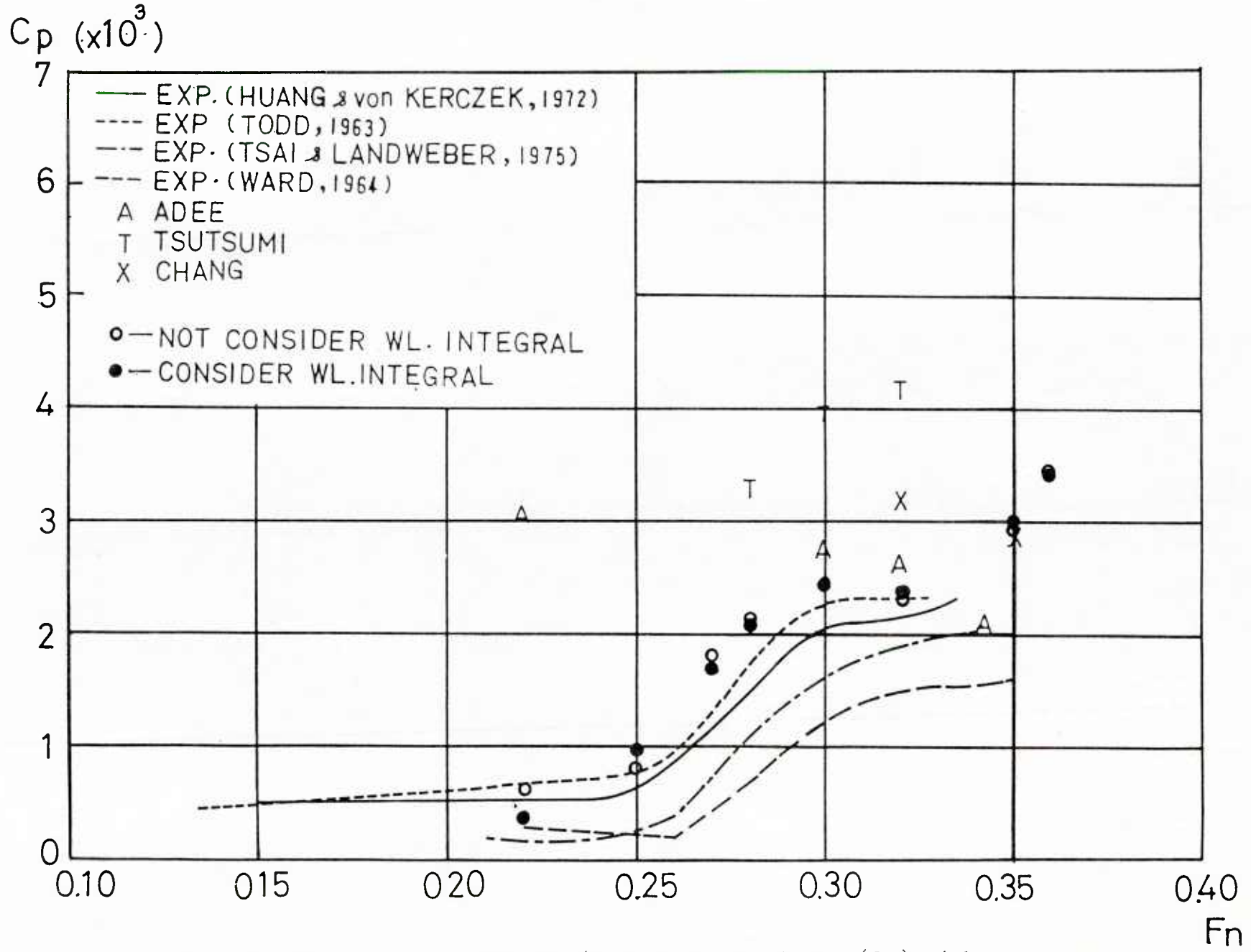

Fig. 18 Comparison of Wave-Resistance Coefficients (Cp) with Experimental and Other Numerical Results for Series 60, C_b=0.6,

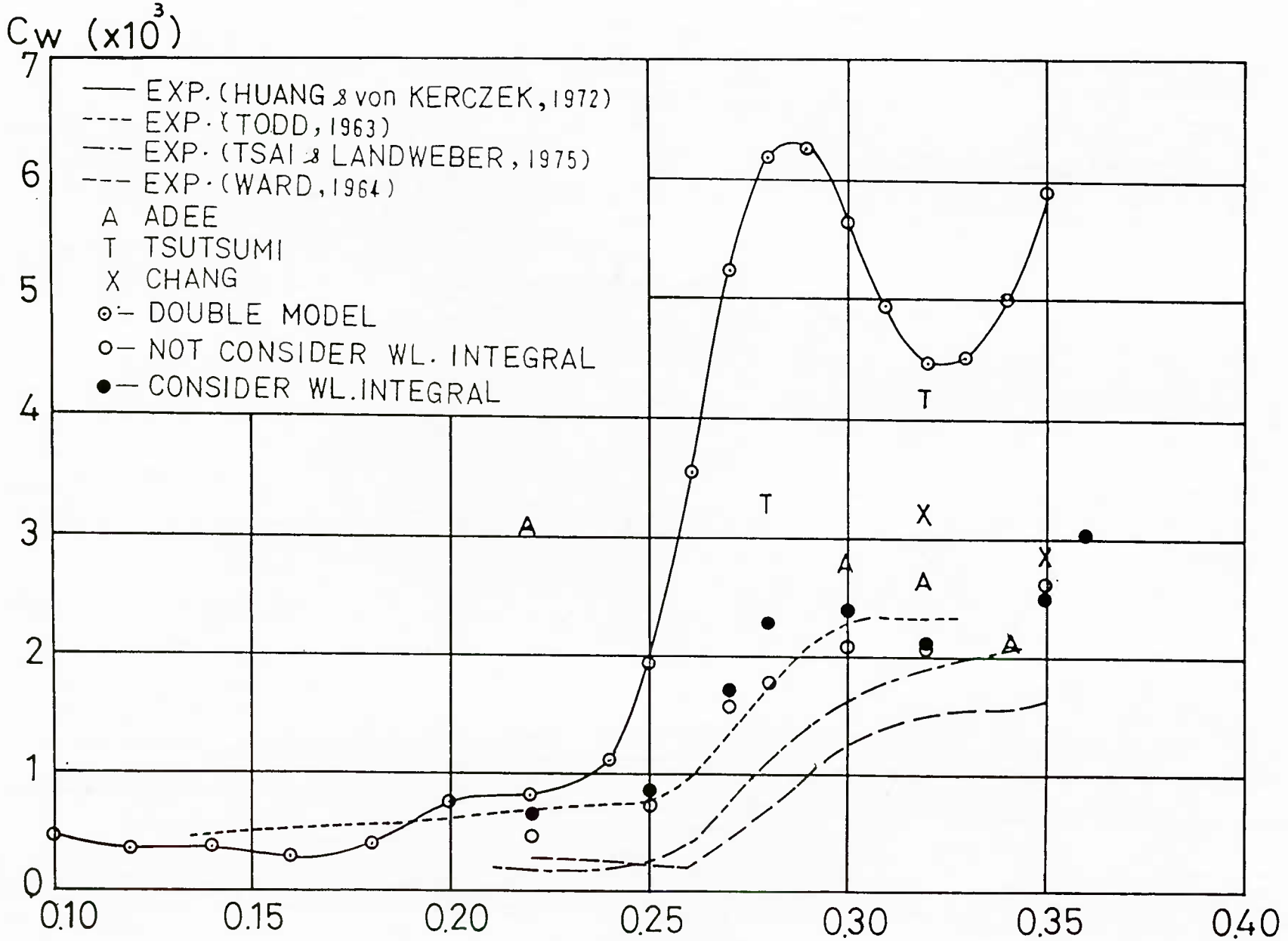

Fig. 19 Comparison of Wave-Resistance Coefficients (Cw) with Experimental and Other Numerical Results for Series 60, C_b=0.6,

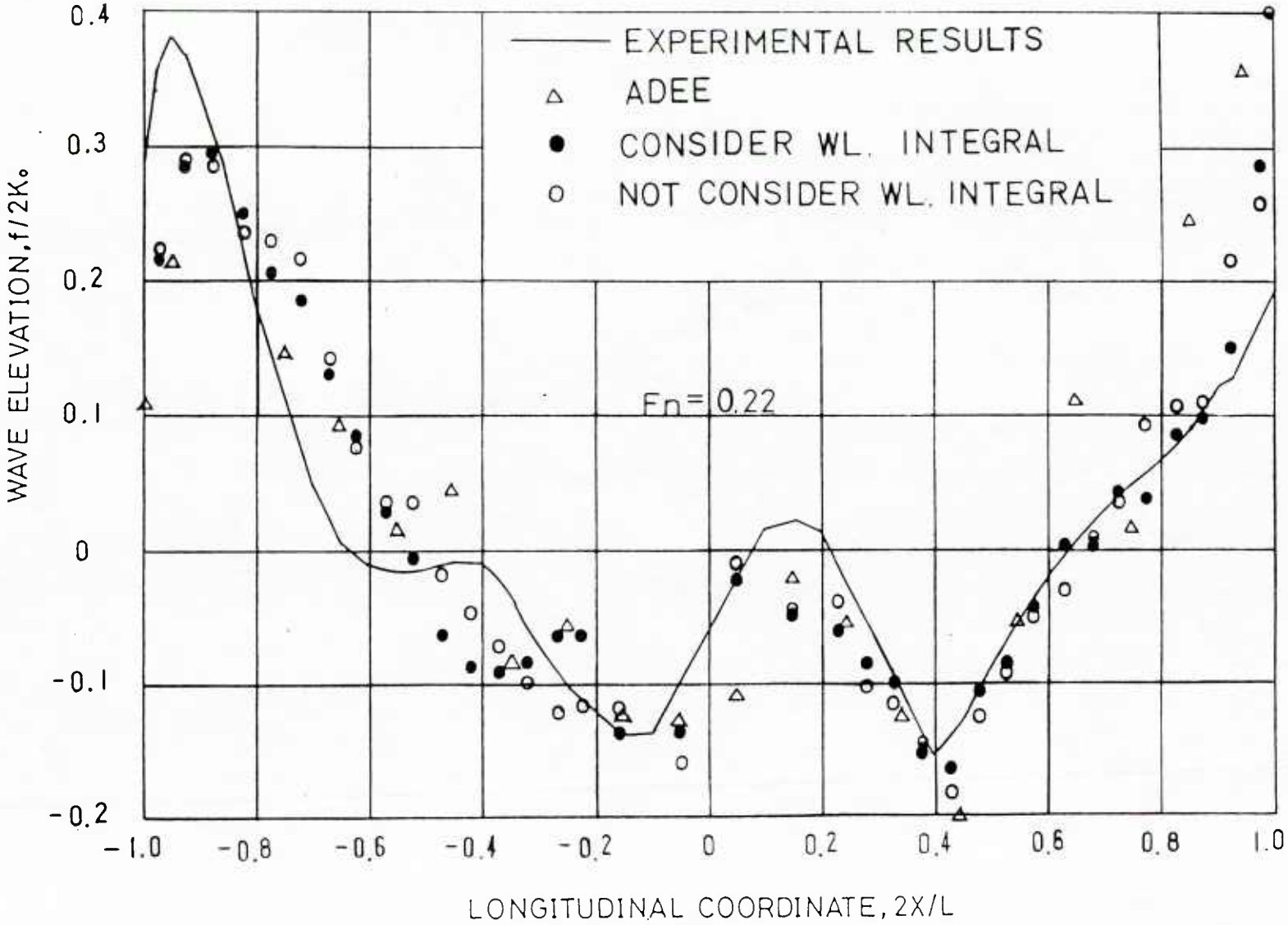

Fig. 20 Comparison of Wave Profile with Experimental and Other Numerical Results for Series 60, C_b=0.6 at Fn=0.22

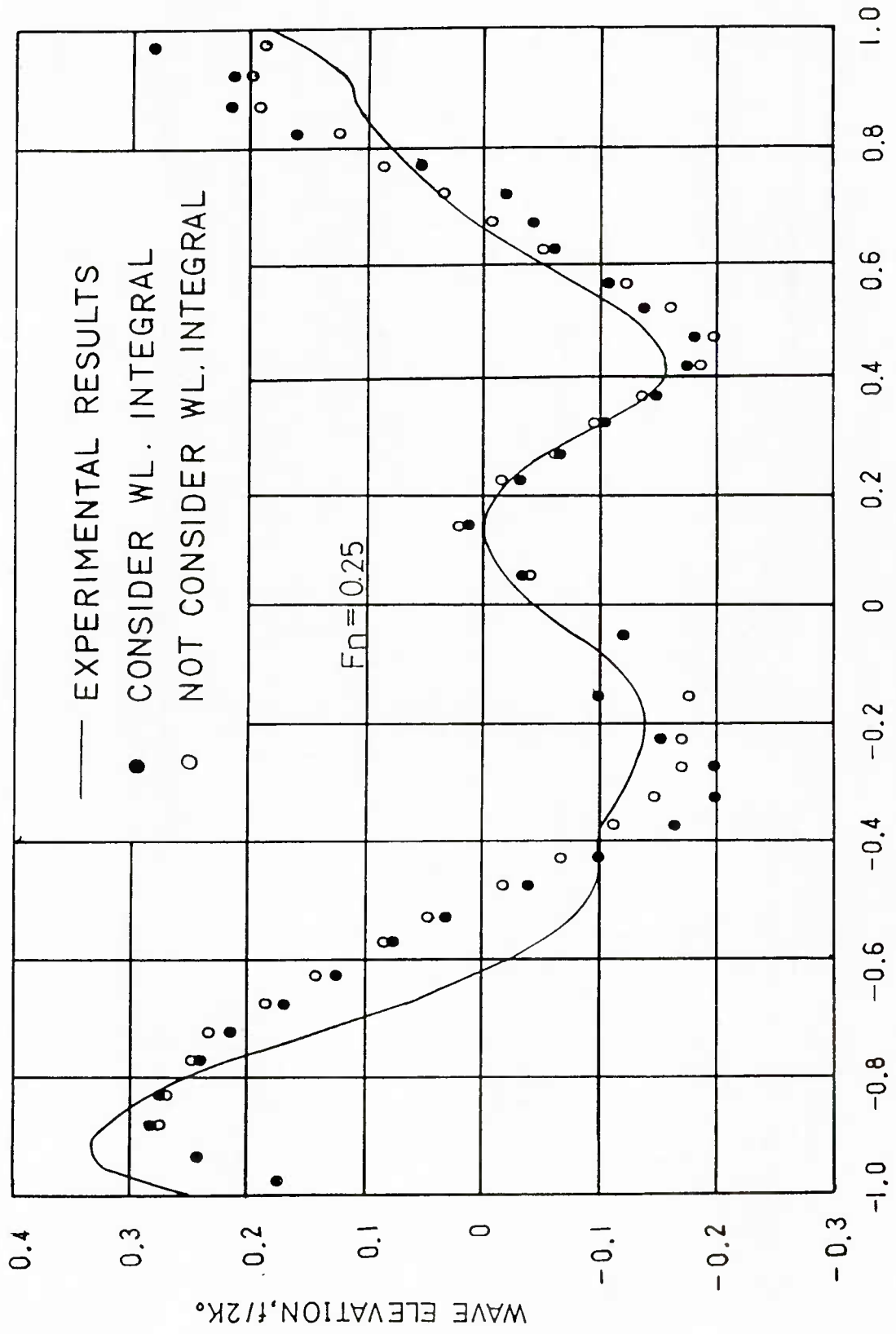

Fig. 21 Comparison of Wave Profile with Experimental Results for Series 60, C_b=0.6 at Fn=0.25

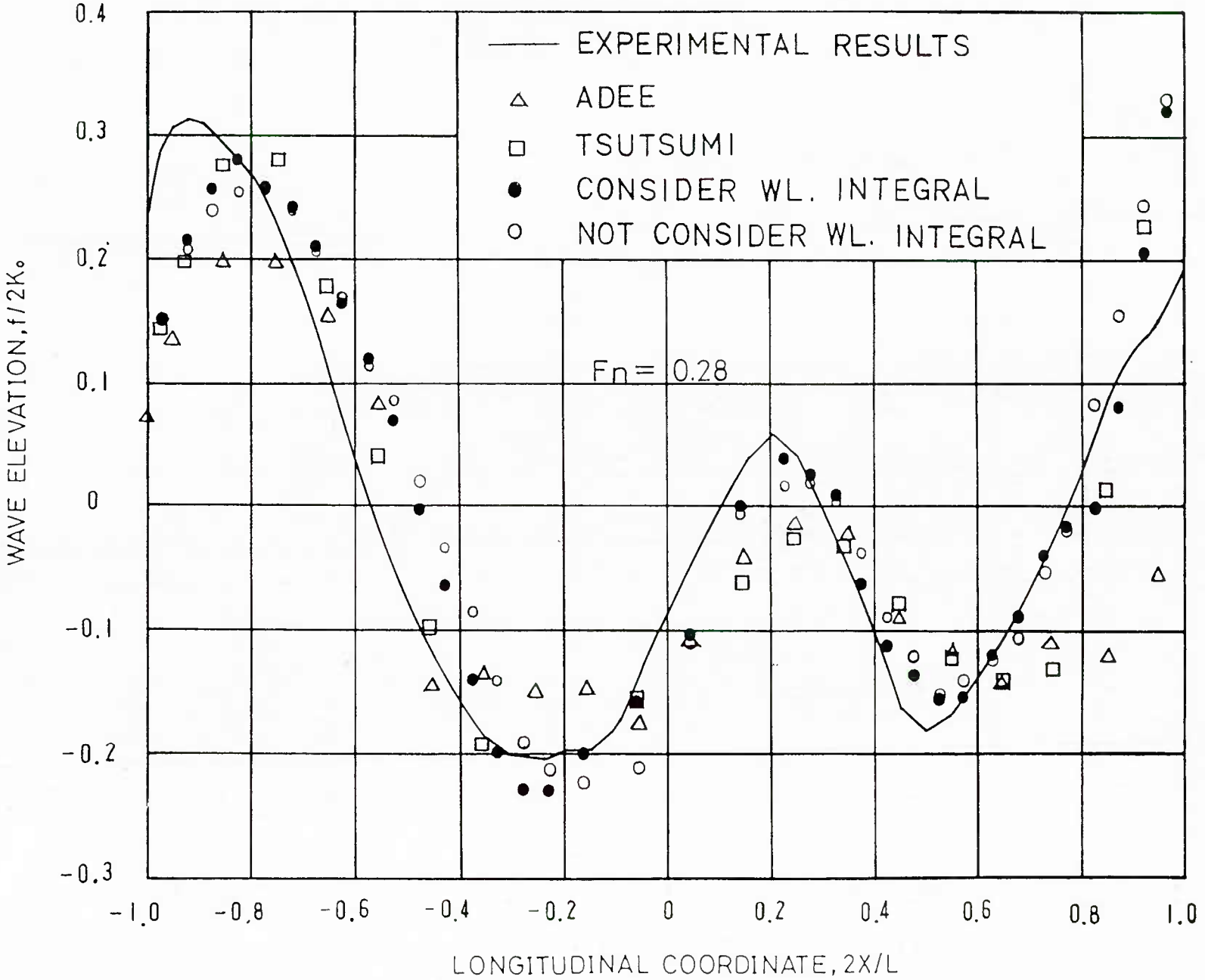

Fig. 22 Comparison of Wave Profile with Experimental and Other Numerical Results for Series 60, C_b=0.6 at Fn=0.28

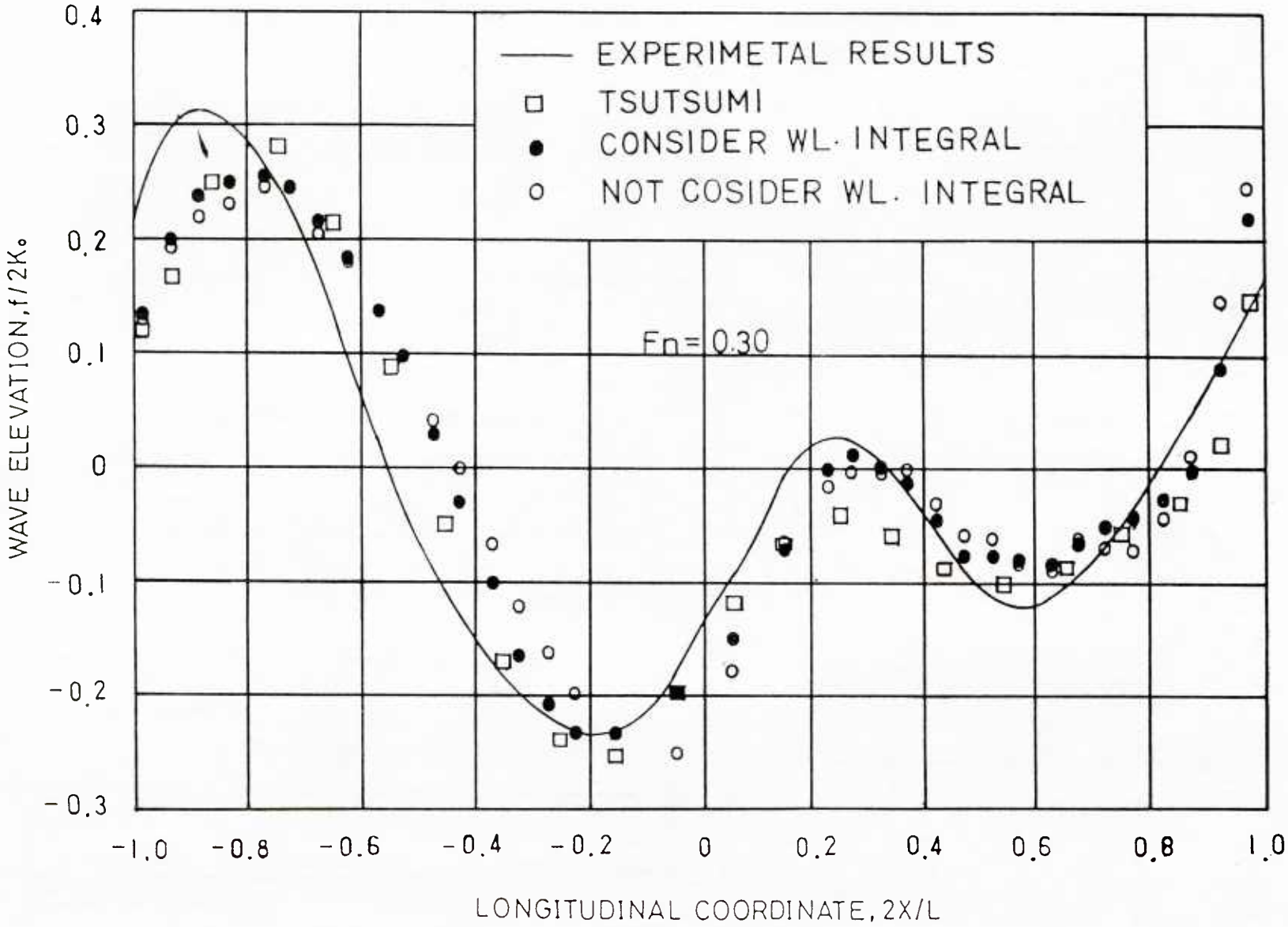

Fig. 23 Comparison of Wave Profile with Experimental and Other Numerical Results for Series 60, C_b=0.6 at Fn=0.30

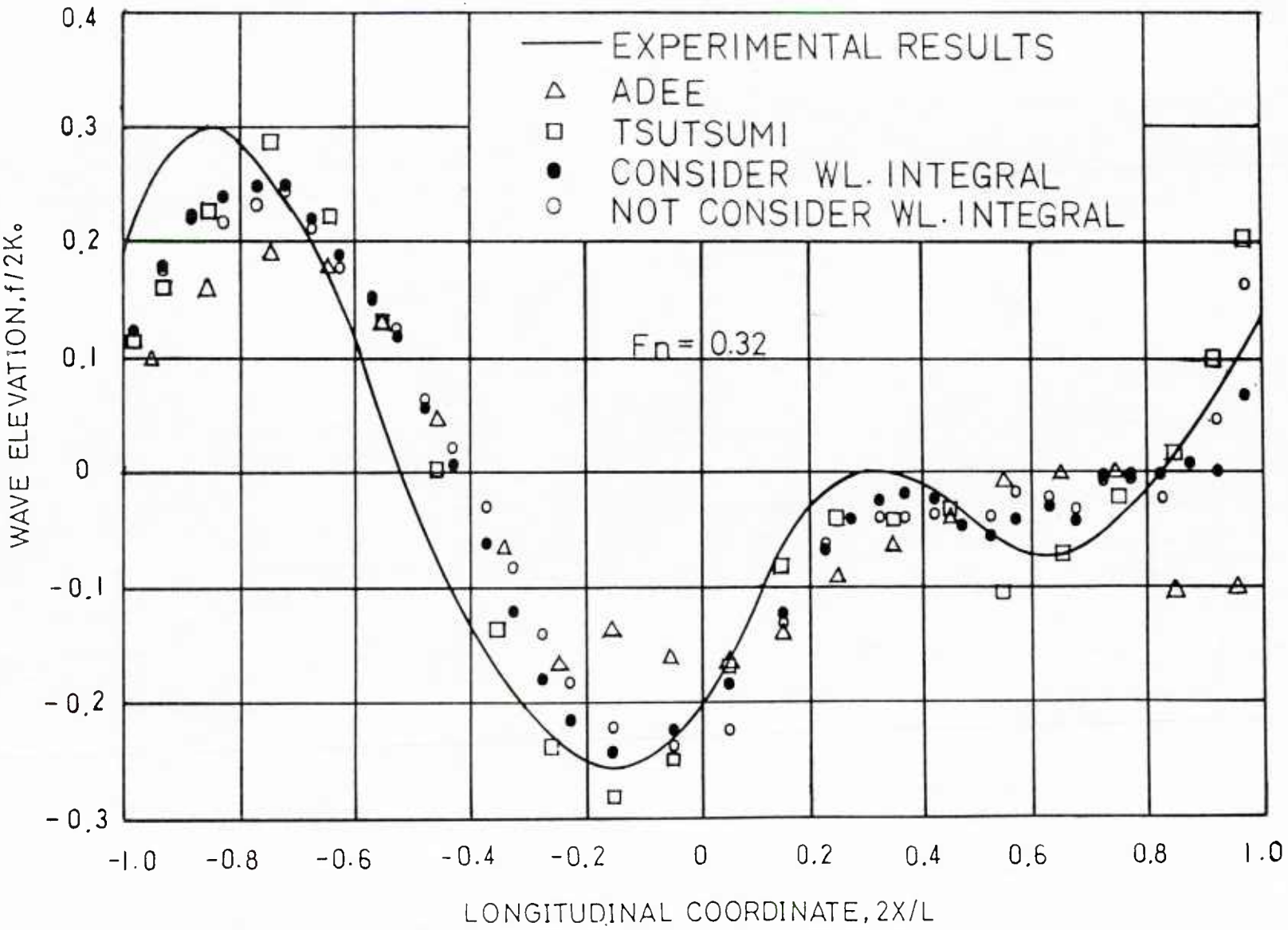

Fig. 24 Comparison of Wave Profile with Experimental and Other Numerical Results for Series 60, C_b=0.6 at Fn=0.32

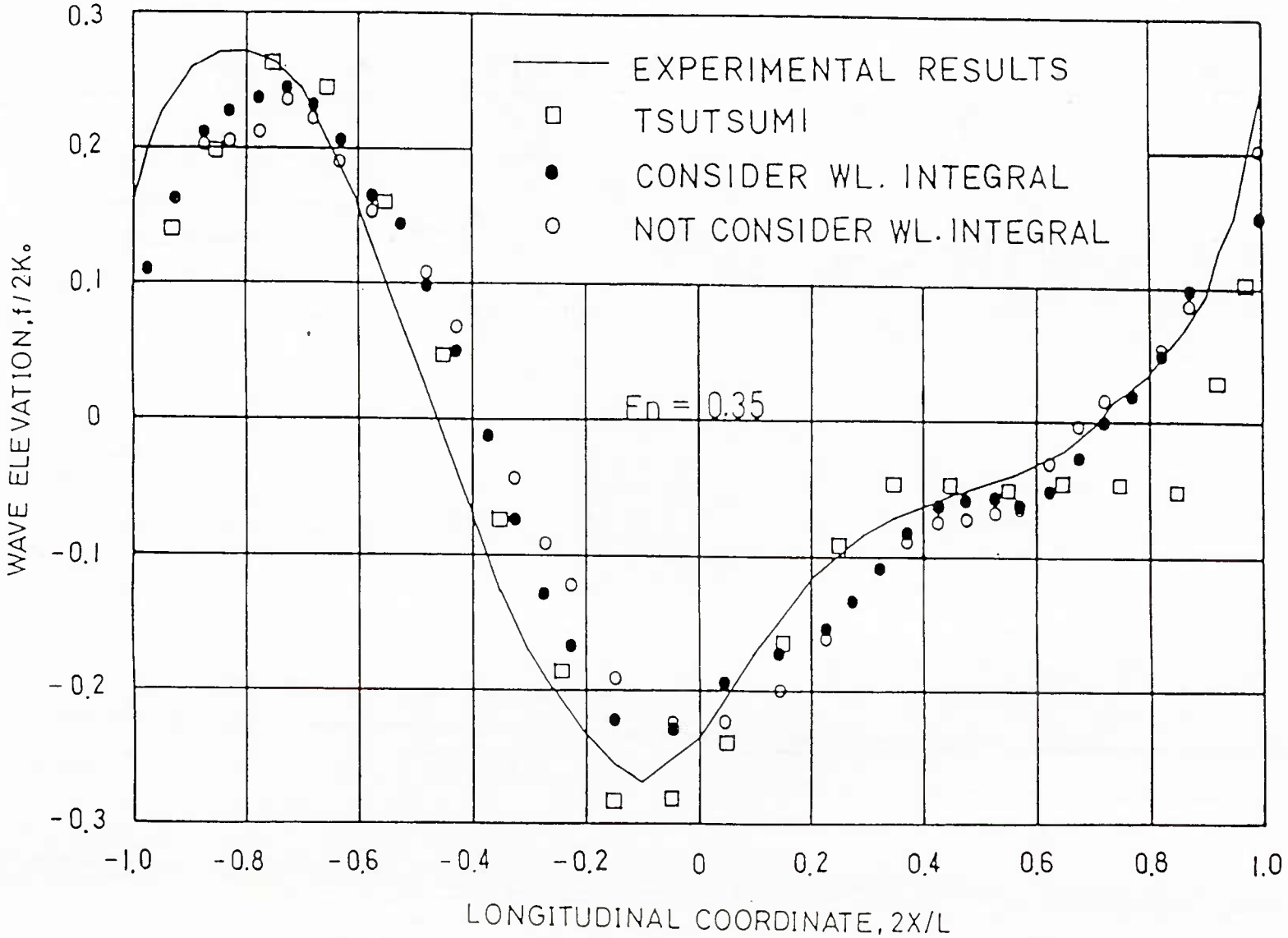

Fig. 25 Comparison of Wave Profile with Experimental and Other Numerical Results for Series 60, C_b=0.6 at Fn=0.35

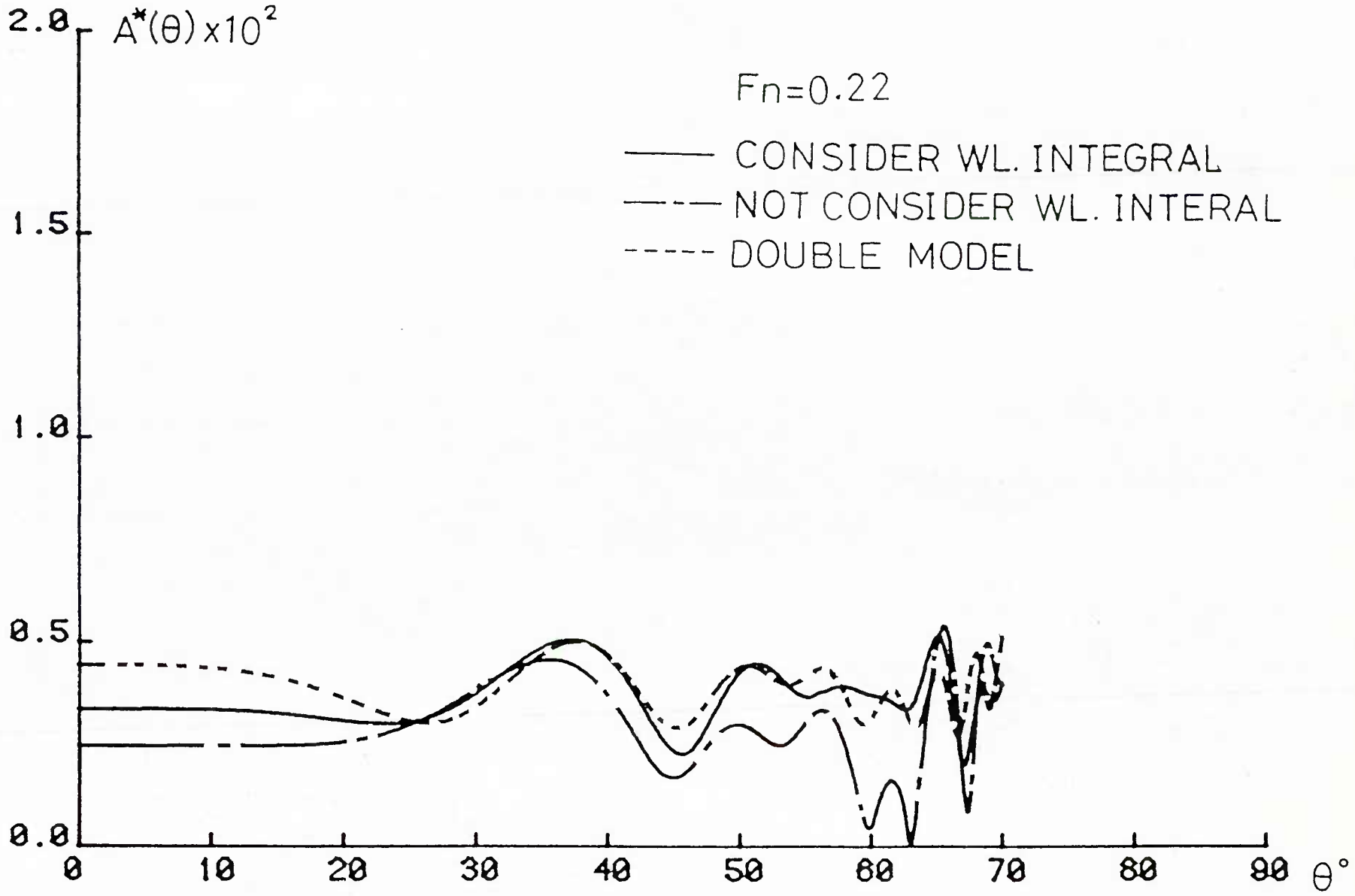

Fig. 26 Amplitude Function of Series 60, C_b=0.6 at Fn=0.22

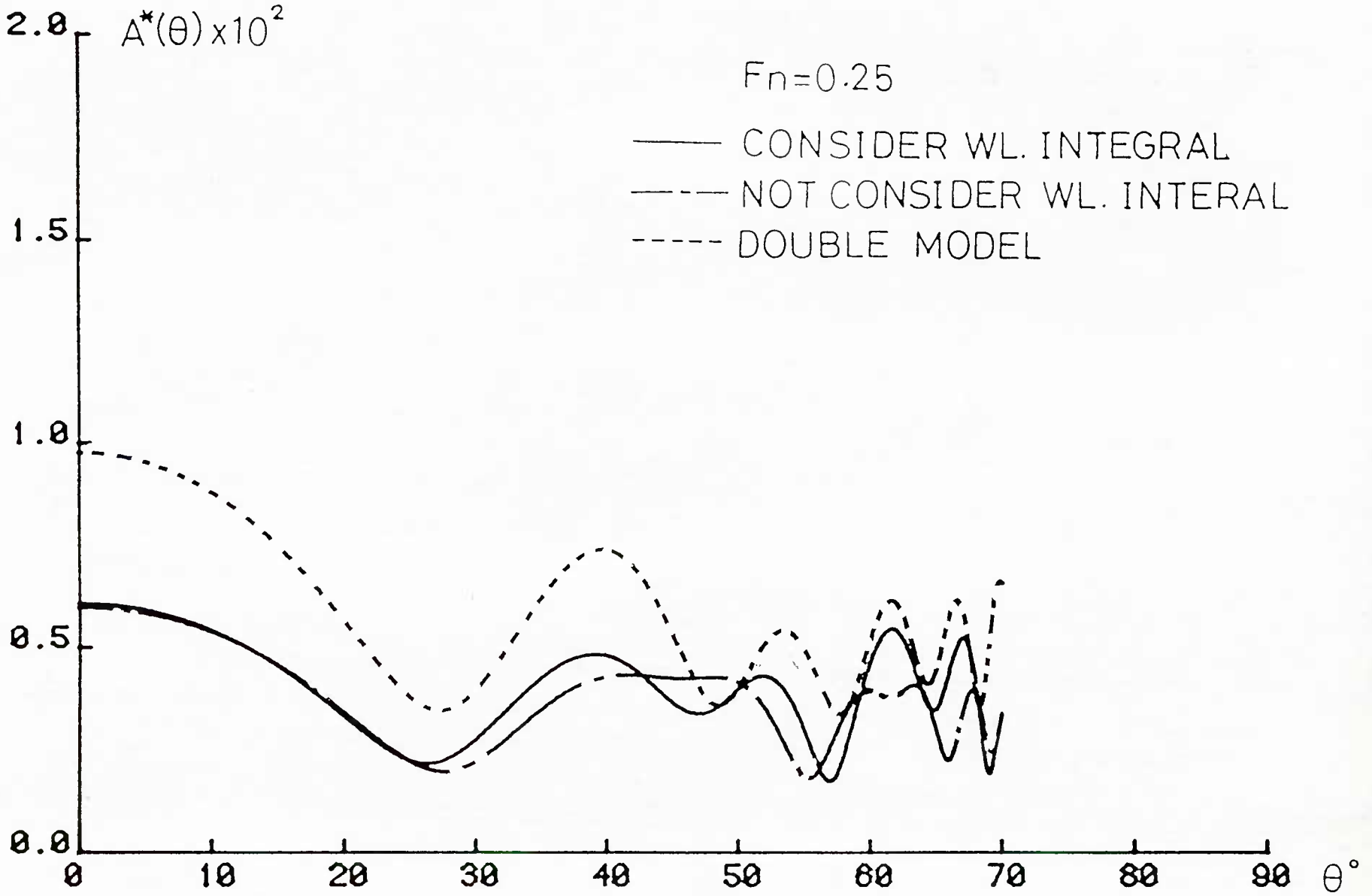

Fig. 27 Amplitude Function of Series 60, C_b=0.6 at Fn=0.25

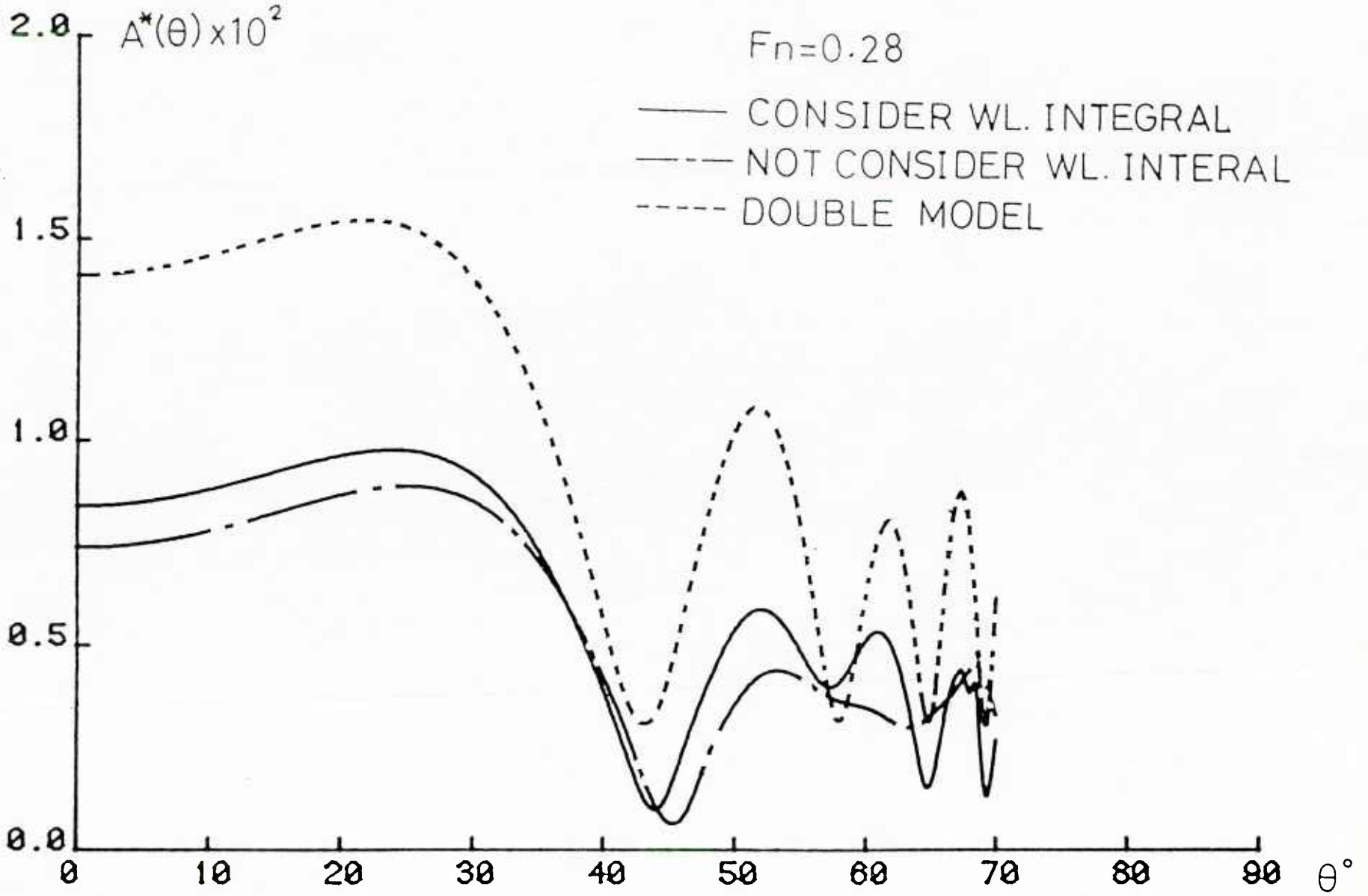

Fig. 28 Amplitude Function of Series 60, C_b=0.6 at Fn=0.28

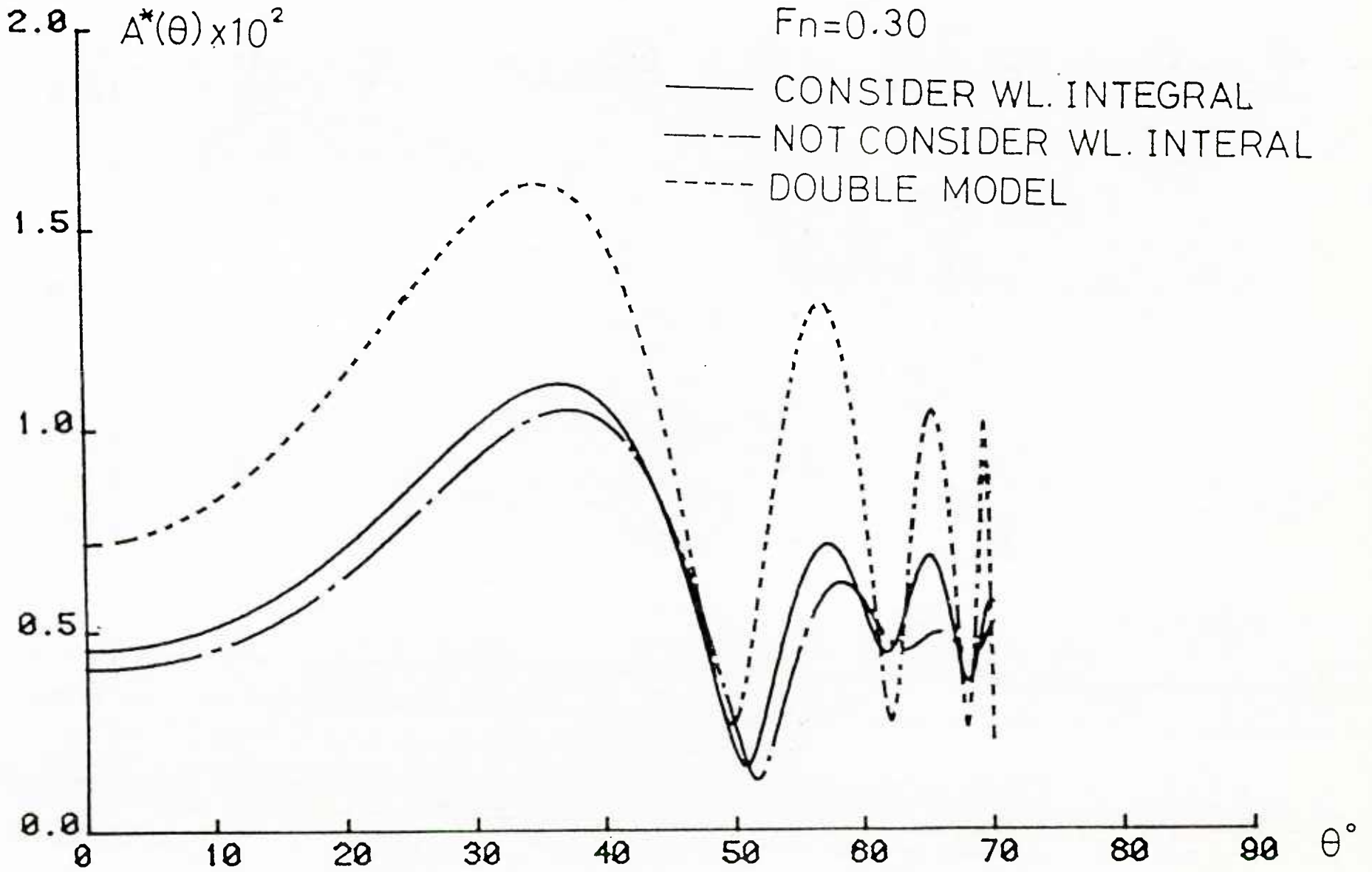

Fig. 29 Amplitude Function of Series 60, C_b=0.6 at Fn=0.30

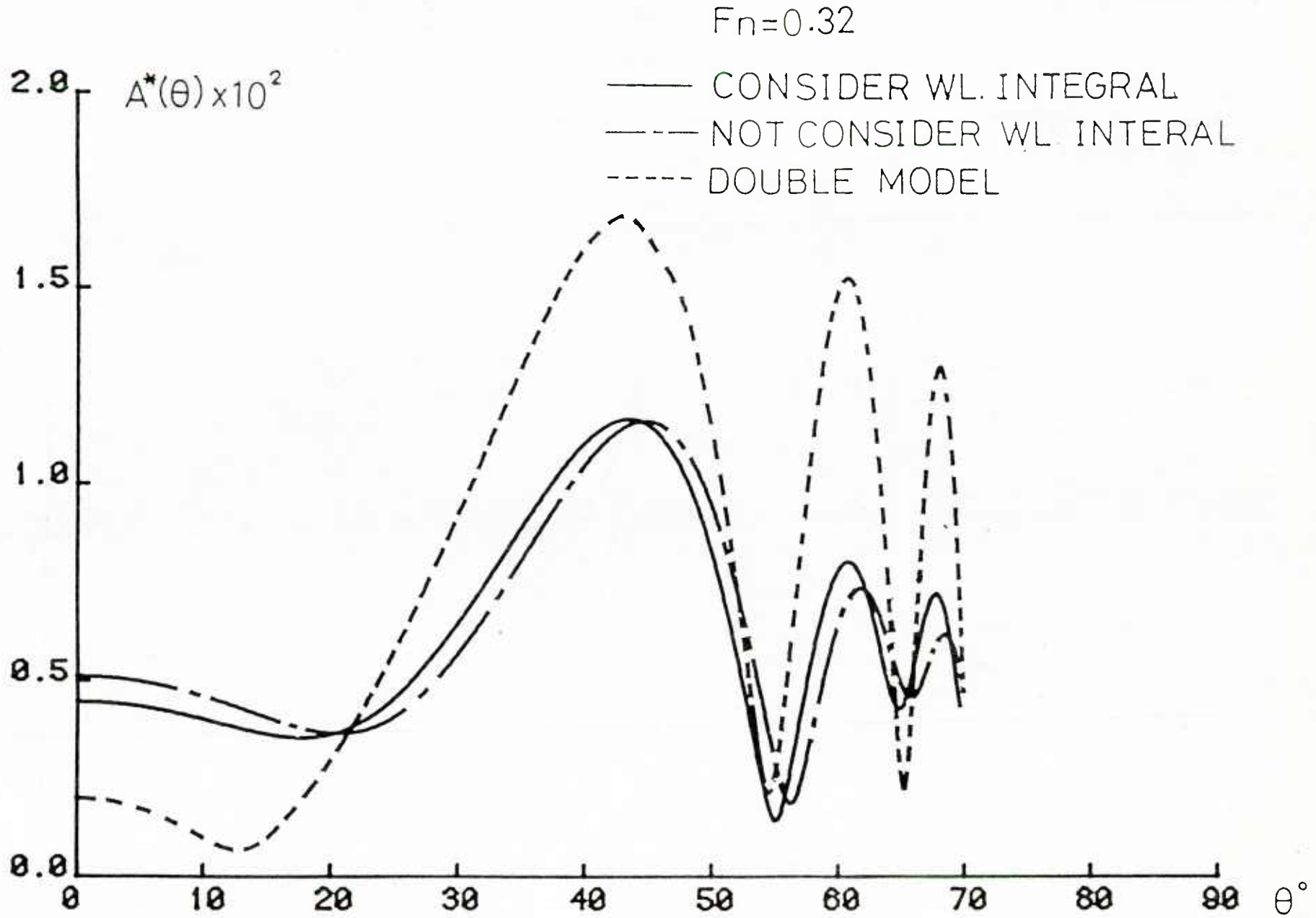

Fig. 30 Amplitude Function of Series 60, C_b=0.6 at Fn=0.32

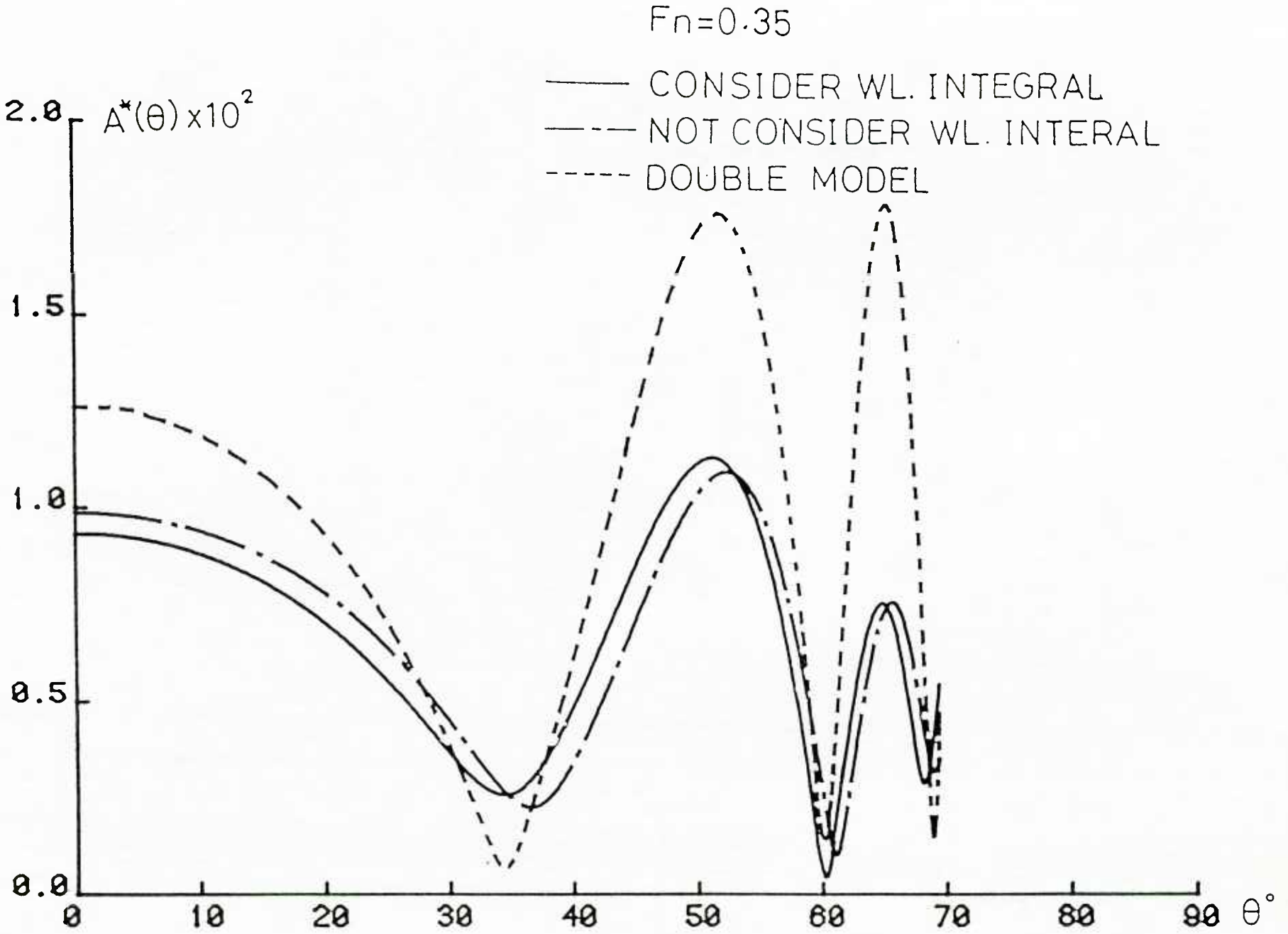

Fig. 31 Amplitude Function of Series 60, C_b=0.6 at Fn=0.35